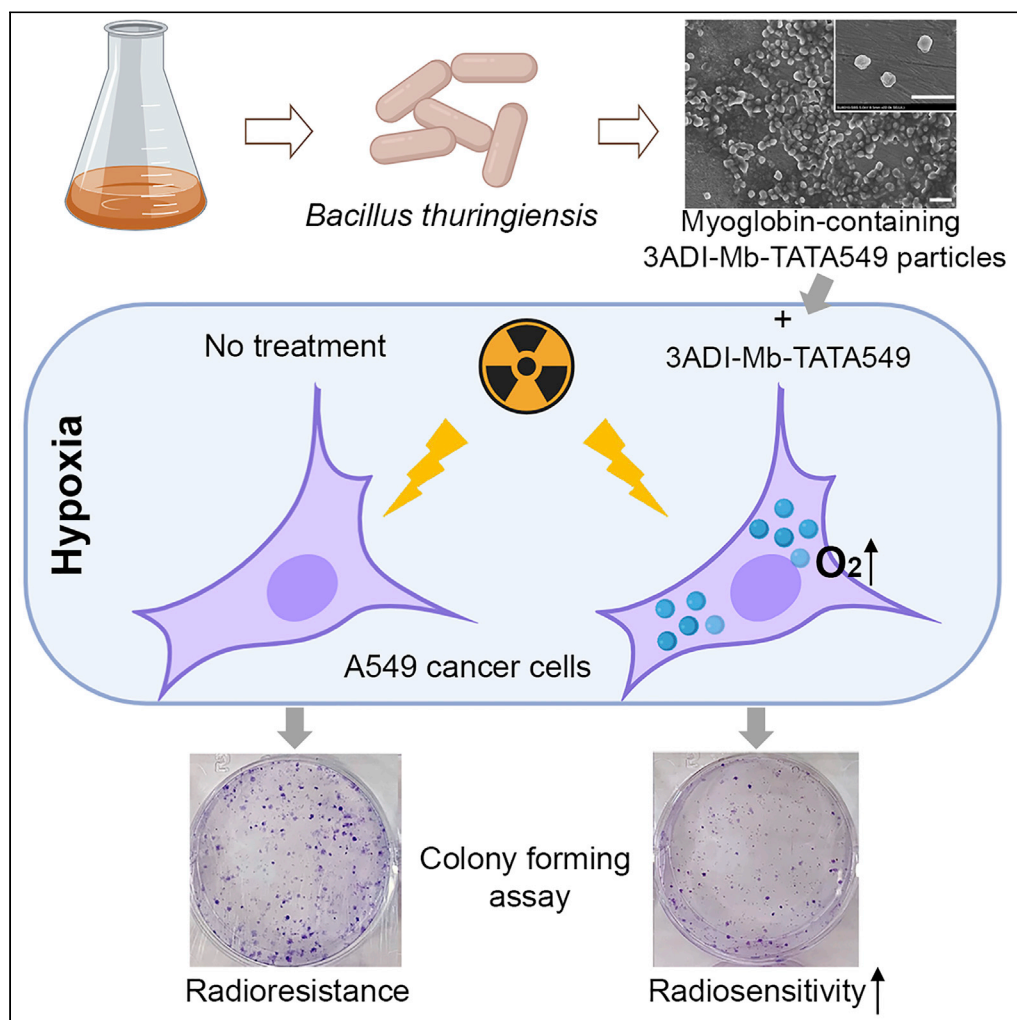


## Article

## Targeted Myoglobin Delivery as a Strategy for Enhancing the Sensitivity of Hypoxic Cancer Cells to Radiation



Zaofeng Yang,  
Bradley S. Heater,  
Clayton T.  
Cuddington,  
Andre F. Palmer,  
Marianne M.M.  
Lee, Michael K.  
Chan

mariannemlee@cuhk.edu.hk  
(M.M.M.L.)  
michaelkchan88@cuhk.edu.hk  
(M.K.C.)

**HIGHLIGHTS**

The N-terminal domain of Cry3Aa can be used to generate sub-micron particles

Genetic fusion of functional peptides to protein particles targets them to A549 cells

Myoglobin is an effective oxygen carrier for delivery of O<sub>2</sub> into hypoxic cancer cells

Targeted myoglobin delivery to hypoxic cancer cells increased their radiosensitivity

Yang et al., iScience 23,  
101158  
June 26, 2020 © 2020 The  
Author(s).  
[https://doi.org/10.1016/  
j.isci.2020.101158](https://doi.org/10.1016/j.isci.2020.101158)

## Article

## Targeted Myoglobin Delivery as a Strategy for Enhancing the Sensitivity of Hypoxic Cancer Cells to Radiation

Zaofeng Yang,<sup>1,3</sup> Bradley S. Heater,<sup>1,3</sup> Clayton T. Cuddington,<sup>2</sup> Andre F. Palmer,<sup>2</sup> Marianne M.M. Lee,<sup>1,\*</sup> and Michael K. Chan<sup>1,4,\*</sup>

## SUMMARY

The effectiveness of cancer radiotherapy is frequently hindered by the hypoxia of the tumor microenvironment. Direct delivery of oxygen to hypoxic tumor tissues is an attractive strategy to overcome this hypoxia-associated radioresistance. Herein, we report the generation of submicron-sized particles comprising myoglobin fused to the crystal-forming domain of Cry3Aa protein for the targeted delivery of oxygen to cancer cells. We demonstrate that myoglobin-containing particles were successfully produced in *Bacillus thuringiensis* with the assistance of the Cry3Aa domain I. Furthermore, these particles could be genetically modified to incorporate the cell penetrating peptide TAT and cell targeting peptide A549.1, resulting in particles that exhibited improved cellular uptake and targeting toward A549 cells. Notably, these myoglobin-containing particles increased the intracellular oxygen levels of A549 cells and thereby sensitized them to radiation. These findings suggest that the targeted delivery of O<sub>2</sub>-bound myoglobin could be an effective approach to enhance the efficacy of radiotherapy.

## INTRODUCTION

Radiotherapy is one of the most important non-surgical modalities for the treatment of cancer. Ionizing radiation used in radiotherapy causes DNA damage because of the production of radicals on cellular DNA and their subsequent oxidation by O<sub>2</sub> (Brown and Wilson, 2004). However, rapid proliferation of cancer cells and the abnormal tumor vasculature lead to hypoxia (Brown and Wilson, 2004; Wilson and Hay, 2011). The lack of O<sub>2</sub> in the hypoxic regions of tumor tissues enables the reduction of DNA free radicals by sulfhydryl-containing compounds, leading to the restitution of DNA and thus cancer cell survival (Brown and Wilson, 2004). Numerous clinical studies have demonstrated a strong correlation between hypoxia and poor response to radiotherapy (Wilson and Hay, 2011). Hence, different strategies have been developed to increase the O<sub>2</sub> levels of tumor tissue, including the reduction of O<sub>2</sub> consumption by metformin, the *in situ* production of O<sub>2</sub> from H<sub>2</sub>O<sub>2</sub>, and the direct delivery of O<sub>2</sub> by oxygen carriers (Cheng et al., 2015; Huang et al., 2016; Li et al., 2017; Luo et al., 2016; Song et al., 2016, 2017a, 2017b). Perfluorocarbons (PFCs) and hemoglobin are two main classes of blood substitutes used for supplying oxygen to tissues during surgery or therapy (Lowe, 2006; Riess, 2006). PFC- or hemoglobin-based nanoparticles have been reported to successfully deliver oxygen to hypoxic tumor sites and improve the efficacy of radio/chemo-therapy (Cheng et al., 2015; Li et al., 2017; Luo et al., 2016; Song et al., 2016, 2017a). However, oxygen dissolves in PFC liquids through loose and non-directional van der Waals interactions, and therefore the oxygen dissolution and release from PFCs is directly proportional to the oxygen tension, making it incapable of releasing O<sub>2</sub> in a hypoxia-dependent manner (Lowe, 2006; Riess, 2006). Similarly, hemoglobin as an oxygen-transport protein has a high p50 for O<sub>2</sub> of 26 mm Hg (half-saturated with O<sub>2</sub> at a pO<sub>2</sub> of 26 mm Hg), which permits the immediate release of bound O<sub>2</sub> to normal tissues (Pratt et al., 2008). Providing an extra supply of O<sub>2</sub> to normal cells is undesirable during radiotherapy, since it can lead to increased DNA damage and thus exacerbate radiation-induced side effects (Barnett et al., 2009). Hence, new O<sub>2</sub> carriers are needed for the controlled release of O<sub>2</sub> to the hypoxic tumor environment.

Myoglobin is a small O<sub>2</sub>-binding protein in vertebrate muscle with a nearly 10-fold lower p50 (2.8 mm Hg) than hemoglobin (Pratt et al., 2008) that appears well suited for potentially achieving a specific

<sup>1</sup>School of Life Sciences and Center of Novel Biomaterials, The Chinese University of Hong Kong, Shatin, Hong Kong SAR, China

<sup>2</sup>Department of Chemical and Biomolecular Engineering, College of Engineering, The Ohio State University, Columbus, OH 43210, USA

<sup>3</sup>These authors contributed equally

<sup>4</sup>Lead contact

\*Correspondence: [marianneemlee@cuhk.edu.hk](mailto:marianneemlee@cuhk.edu.hk) (M.M.M.L.), [michaelkchan88@cuhk.edu.hk](mailto:michaelkchan88@cuhk.edu.hk) (M.K.C.)

<https://doi.org/10.1016/j.isci.2020.101158>



	Cry3Aa	Cry3AaDI	Mb	3A-Mb	3ADI-Mb
Molecular weight (kDa)	73.11	33.37	17.33	90.56	50.83
Mb loading capacity				19.14%	34.09%

**Table 1. Myoglobin (Mb) Loading Capacity of 3A-Mb versus 3ADI-Mb**

Loading capacity is defined as the mass ratio of Mb to 3A-Mb or 3ADI-Mb.

hypoxia-responsive release of O<sub>2</sub>. We thus surmised that the delivery of O<sub>2</sub>-bound myoglobin could be a viable strategy to specifically increase O<sub>2</sub> levels in hypoxic cancer cells. Nevertheless, the direct delivery of free proteins is challenging owing to their instability and low cell penetration efficiency (Mitrugotri et al., 2014; Sun et al., 2014). Various materials, like polymers, lipids, inorganic materials, and proteins, have been utilized to manufacture nano/micro-carriers with different chemical and physical properties to protect cargo proteins from degradation and effectively deliver them into mammalian cells (Gu et al., 2011; Sun et al., 2014). Compared with other materials, protein-based carriers have certain advantages, including good biocompatibility, biodegradability, and ease of modification (Gu et al., 2011; Qin et al., 2019).

We have previously described a protein/peptide delivery platform based on Cry3Aa protein that naturally forms sub-micrometer-sized crystalline inclusions within the bacterium *Bacillus thuringiensis* (Bt) (Nair et al., 2015; Yang et al., 2019). This Cry platform has shown to considerably improve the stability of its cargo protein in the form of Cry3Aa-cargo fusion protein crystal (Heater et al., 2018, 2019; Nair et al., 2015). In the present study, we demonstrate that the N-terminal helical domain I of Cry3Aa protein (3ADI) can be used in a related way to promote the formation of 3ADI-myoglobin (3ADI-Mb) fusion protein inclusions directly within Bt cells. After coupling with TAT cell penetrating peptide and A549.1 targeting peptide, the resultant 3ADI-myoglobin-TATA549 (3ADI-Mb-TATA549) protein particles exhibited significantly improved cellular uptake and targeting efficiency toward non-small cell lung cancer A549 cells. Notably, the delivery of O<sub>2</sub>-bound myoglobin mediated by the 3ADI-Mb-TATA549 platform increased the intracellular O<sub>2</sub> levels of hypoxic A549 cells, thereby enhancing their susceptibility to radiation.

## RESULTS

### Production and Characterization of 3A-Mb and 3ADI-Mb

Our initial studies began with a fusion of myoglobin to the full-length Cry3Aa protein. These Cry3Aa-myoglobin (3A-Mb) fusion protein crystals were produced in Bt strain 407-OA (Lereclus et al., 1995) and isolated by sucrose density gradient centrifugation. SDS-PAGE analysis of the isolated crystals revealed a major band between 75 and 100 kDa, in agreement with the predicted 90.56 kDa molecular weight of the 3A-Mb fusion protein (Figures S1 and S2A). The UV-vis absorption spectrum of the 3A-Mb crystals showed a Soret peak at 416 nm and two Q bands at 541 and 579 nm, which are indicative of an O<sub>2</sub>-bound myoglobin (MbO<sub>2</sub>) (Figure S2B). The spectrum was identical to that of the free MbO<sub>2</sub> protein (Figure S2C).

Having shown that the resultant Cry3Aa-myoglobin fusion crystals retained their O<sub>2</sub>-binding capacity, we then sought to maximize the Mb payload since high loading capacity is a key and desirable feature in drug delivery systems. Park and Federici had previously shown that the N-terminal helical domain I of Cry3Aa (3ADI) was responsible for its crystallization in Bt cells (Park and Federici, 2000). We thus hypothesized that the fusion of myoglobin to this domain might allow for the production of 3ADI-Mb protein inclusions with a higher Mb payload than 3A-Mb (Table 1 and Figure S1). As predicted, 3ADI-Mb protein inclusions were successfully produced in and purified from Bt (Figures 1A and 1B). Scanning electron micrographs (SEMs) revealed that the purified 3ADI-Mb inclusions were sphere-like particles with an average diameter of 869.22 nm (Figure 1B). Consistent with the SEM measurements, dynamic light scattering (DLS) analysis indicated that the purified 3ADI-Mb protein particles were uniform (PDI = 0.141) with a mean hydrodynamic diameter of 886.3 nm (Figure 1C). The average zeta potential of the 3ADI-Mb at -9.94 mV (Figure 1D) suggested that these bioparticles possessed a slightly negatively charged surface. To ascertain whether the cargo Mb protein was correctly folded within the 3ADI-Mb framework, the O<sub>2</sub>-binding ability of 3ADI-Mb particles was examined by UV-vis absorption. Similar to the spectra of 3A-Mb (Figure S2B) and free MbO<sub>2</sub> protein (Figure S2C), an intense peak in the Soret region and two Q-band peaks at 542 and 580 nm were also observed for 3ADI-Mb particles (Figure 1E), thus verifying the presence of bound O<sub>2</sub>.

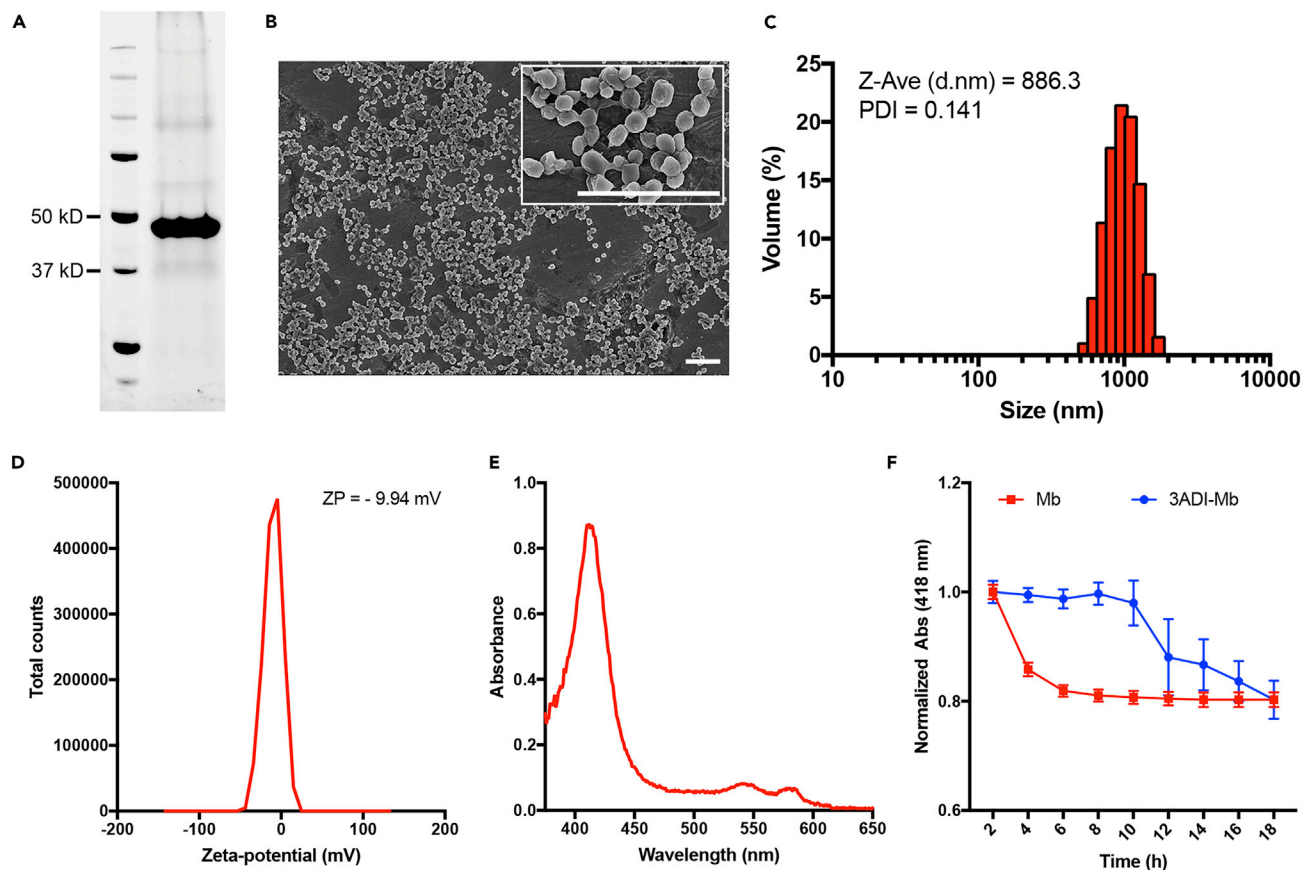


**Figure 1. Characterization of 3ADI-Mb Protein Particle and Its Stability**

- (A) SDS-PAGE analysis of purified 3ADI-Mb protein particles.  
(B) SEM images of purified 3ADI-Mb showing their uniformity in size and shape. Scale bar, 5  $\mu\text{m}$ .  
(C) Size distribution of 3ADI-Mb determined by DLS.  
(D) Zeta potential distribution of 3ADI-Mb.  
(E) UV-vis absorption spectra of 3ADI-Mb protein particles.  
(F) Denaturation profiles of Mb protein and 3ADI-Mb protein particles. Data are presented as mean  $\pm$  standard error of the mean.

### Stability of 3ADI-Mb Protein Particles

One important feature of any drug delivery system, particularly for peptide- or protein-based therapeutics, is the ability of the carriers to confer protection to their cargos. We have previously demonstrated that the framework of Cry3Aa could enhance the stability of its protein cargo (Heater et al., 2018, 2019; Nair et al., 2015; Yang et al., 2019). We therefore hypothesized that the 3ADI-Mb particle should also be able to stabilize its fused Mb partner. To confirm this hypothesis, 3ADI-Mb particles and Mb protein were incubated in PBS at 37°C for 18 h, and their absorbance at 418 nm ( $\text{Abs}_{418}$ ) was measured to monitor the protein denaturation (Hargrove and Olson, 1996; Sykes et al., 1999). As shown in Figure 1F, significant denaturation of the free Mb protein was observed within 4 h post incubation, and after 8 h, the free Mb protein was almost completely denatured. In contrast, the  $\text{Abs}_{418}$  of 3ADI-Mb particles remained stable during the first 10 h suggesting only minimal denaturation. Thus, similar to Cry3Aa crystals, the 3ADI framework could enhance the stability of its cargo Mb protein, making it well suited for delivering Mb protein to mammalian cells.

### Evaluation of the A549.1 Targeting Peptide

The use of traditional radiotherapy or chemotherapy to treat cancer is frequently limited by its serious side effects that arise from the toxicity of non-selective therapeutics to normal cells or tissues (Allen, 2002; Barnett et al., 2009). Tumor targeting via the coupling of targeting ligands, such as small molecules, antibodies, and peptides, to the surface of drug carriers has been shown to be effective in improving cell recognition and cellular uptake, resulting in enhanced specificity and improved efficacy toward cancer cells

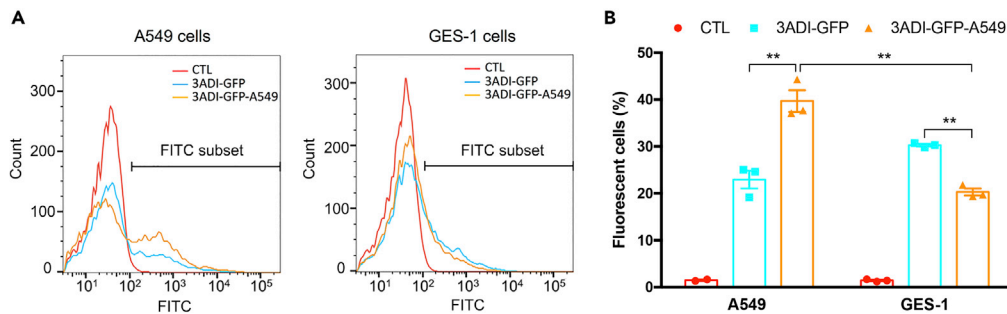


**Figure 2. Evaluation of the Targeting Efficiency of A549.1 Peptide**

(A) Representative flow cytometric histograms of A549 cells (left) and GES-1 cells (right) treated with 3ADI-GFP or 3ADI-GFP-A549 protein particles.

(B) Percentage of fluorescent cells.

Data are presented as mean  $\pm$  standard error of the mean. \*\*p < 0.01.

(Allen, 2002; Danhier, 2016). One advantage of protein-based carriers is the ease of manipulation via genetic modification to accommodate ligands or motifs for specific purposes. Consequently, we appended a known targeting peptide A549.1 (McGuire et al., 2014) specific for human non-small cell lung cancer (NSCLC) A549 cells via genetic fusion to the C terminus of 3ADI-GFP to test whether such approach could indeed promote enhanced selectivity toward lung cancer cells. Purified 3ADI-GFP or 3ADI-GFP-A549 particles were incubated with either A549 or normal GES-1 cells for 24 h, and their binding efficiency and specificity were assessed using flow cytometry. As shown in Figure 2, 3ADI-GFP-A549 particles exhibited preferential binding to A549 cells in comparison with 3ADI-GFP. Intriguingly, the presence of A549.1 peptide appeared to reduce the non-specific binding of 3ADI-GFP particles to the normal GES-1 cells (Figure 2), further supporting the notion that the A549.1 peptide could aid in facilitating the selectivity of Cry protein-based particles toward A549 cells.

### Modification of 3ADI-Mb with Functional Peptides

Given the promising results obtained for 3ADI-GFP-A549 particles, we thus proceeded to modify 3ADI-Mb similarly to generate a 3ADI-Mb-A549 construct with potentially enhanced selectivity toward A549 cells. This construct was further modified for cell internalization since previous studies from our laboratory had shown that the related Cry3Aa protein crystals could not be easily taken up by non-phagocytic cells (Yang et al., 2019). Hence, the known cell penetrating peptide TAT (Frankel and Pabo, 1988; Green and Loewenstein, 1988) was introduced upstream of the targeting peptide A549.1 to generate the 3ADI-Mb-TATA549 construct (Figure S1). To assess the impact of these peptides on the functional properties of their respective constructs, 3ADI-Mb, 3ADI-Mb-A549, and 3ADI-Mb-TATA549 particles were produced in *Bt* cells, labeled with Alexa Fluor 488, and their targeting specificities and cellular uptake efficiencies were evaluated. Consistent with the results for 3ADI-GFP-A549, incorporation of the A549.1 targeting peptide enhanced the binding of 3ADI-Mb-A549 and 3ADI-Mb-TATA549 particles toward A549 cells, as verified by flow cytometric analysis (Figures 3A–3C). Moreover, cells treated with Alexa Fluor 488-labeled 3ADI-Mb-TATA549 particles exhibited significantly higher mean fluorescence intensities (Figure 3C), suggesting more particles were being delivered to A549 cells. We surmised that the increase was due to the ability of the cell penetrating TAT peptide aiding in the cellular internalization of the 3ADI-Mb-TATA549 particles. This conjecture was confirmed by confocal microscopy, which revealed the facile uptake of 3ADI-Mb-TATA549 particles by A549 cells, but not 3ADI-Mb and 3ADI-Mb-A549 particles, which were found predominately on the membrane surface of the cells (Figure 3D).

### 3ADI-Mb-TATA549 Particles Enhanced the Radiosensitivity of the Hypoxia-Induced Radioresistant A549 Cells

Since 3ADI-Mb-TATA549 protein particles were significantly more efficient at targeting and entering A549 cancer cells, this construct was further characterized and used for subsequent experiments (Figure 4). Purified 3ADI-Mb-TATA549 particles retained the red color of Mb, and their purity was confirmed by SDS-PAGE analysis (Figures 4A and 4B). SEM images showed that purified 3ADI-Mb-TATA549 inclusions were uniform sphere-like particles with an average diameter of 647.71 nm (Figure 4C). DLS and zeta potential measurements indicated that these particles have an average hydrodynamic diameter of 630.4 nm (PDI = 0.186) and a negatively charged surface (ZP =  $-10.7$  mV) (Figures 4E and S3A), respectively. The

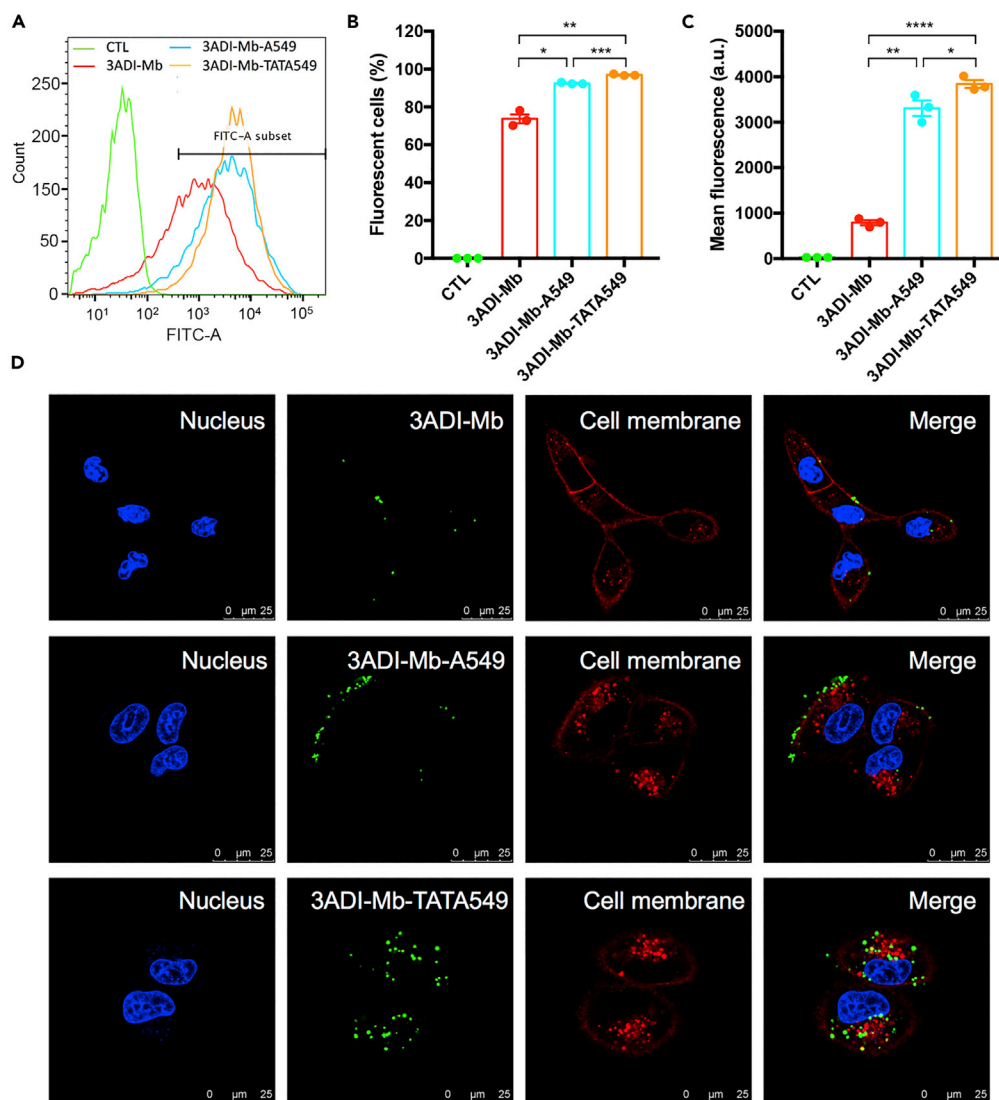


**Figure 3. Cell Targeting and Cellular Uptake of 3ADI-Mb-TATA549 Protein Particles**

(A) Representative flow cytometric histograms of A549 cells treated with Alexa Fluor 488-labeled 3ADI-Mb, 3ADI-Mb-A549, or 3ADI-Mb-TATA549 protein particles.

(B and C) (B) Percentage of fluorescent cells and (C) mean fluorescence intensity of A549 cells with different treatment. (D) Confocal images showing the targeting ability and uptake efficiency of Alexa Fluor 488-labeled 3ADI-Mb, 3ADI-Mb-A549, and 3ADI-Mb-TATA549 particles. Scale bar, 25  $\mu$ m.

Data in 3B and 3C are presented as mean  $\pm$  standard error of the mean. \* $p < 0.05$ ; \*\* $p < 0.01$ ; \*\*\* $p < 0.001$ ; \*\*\*\* $p < 0.0001$ .

O<sub>2</sub>-bound state of 3ADI-Mb-TATA549 particles was confirmed by its UV-vis absorption spectrum (Figure 4G) and further verified by its O<sub>2</sub> dissociation curve generated using a HEMOX analyzer. The O<sub>2</sub> dissociation curve of 3ADI-Mb-TATA549 protein particles was hyperbolic similar to that of the free Mb protein indicating O<sub>2</sub> binding (Figure S4). Furthermore, the 3ADI-Mb-TATA549 particles exhibited a  $p50$  value (2.593 mm Hg) comparable with that of wild-type Mb protein ( $p50 = 3.319$  mm Hg), suggesting that the ability to bind and release O<sub>2</sub> of the fused Mb within the particle was not affected. Moreover, stability studies shown that 3ADI-Mb-TATA549 protein particles still exhibited higher stability than free Mb protein after peptide modifications (Figure S5).

In preparation for studies of the 3ADI-Mb-TATA549-mediated delivery of O<sub>2</sub> to A549 cells, a construct 3ADI-MbH97D-TATA549 harboring a H97D mutation in its Mb domain was produced to be used as a

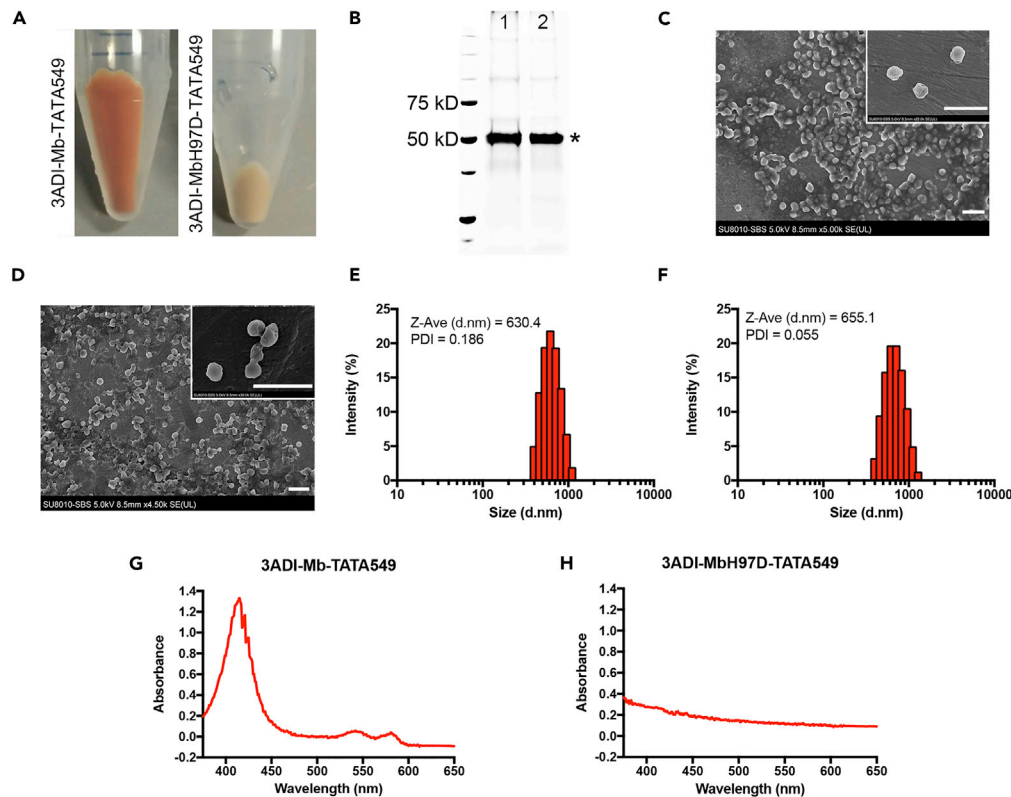


**Figure 4. Characterization of 3ADI-Mb-TATA549 and 3ADI-MbH97D-TATA549 Protein Particles**

(A) Color difference showing the heme binding to 3ADI-Mb-TATA549, but not 3ADI-MbH97D-TATA549 particles.

(B) SDS-PAGE analysis of 3ADI-Mb-TATA549 (lane 1) and 3ADI-MbH97D-TATA549 (lane 2) particles. The asterisk indicates the protein bands of these two particles.

(C and D) SEM images of (C) 3ADI-Mb-TATA549 and (D) 3ADI-MbH97D-TATA549 protein particles. Scale bar, 2  $\mu$ m.

(E and F) Size distributions of (E) 3ADI-Mb-TATA549 and (F) 3ADI-MbH97D-TATA549 protein particles determined by DLS.

(G and H) UV-vis absorption spectra of (G) 3ADI-Mb-TATA549 and (H) 3ADI-MbH97D-TATA549 particles.

background control to eliminate any possible particle effects. This H97D Mb mutation has been reported to promote heme dissociation (Hargrove and Olson, 1996) and thus loss of O<sub>2</sub>-binding ability. DLS analysis of the purified 3ADI-MbH97D-TATA549 protein inclusions showed similar size (hydrodynamic diameter of 655.1 nm) and surface charge (ZP = -10.6 mV) compared with their wild-type counterparts (Figures 4D, 4F, and S3B and Table S1). However, unlike the wild-type 3ADI-Mb-TATA549, these particles did not possess the red color associated with heme binding, suggesting their loss of heme ligand and therefore the inability to bind O<sub>2</sub> (Figures 4A and 4H).

To validate the 3ADI-Mb-TATA549-mediated cellular delivery of O<sub>2</sub>, A549 cells were incubated with free Mb protein, 3ADI-MbH97D-TATA549 or 3ADI-Mb-TATA549 particles at 37°C under 1.5% O<sub>2</sub> (hypoxia) for 6 h. The relative intracellular O<sub>2</sub> level was determined using the Hypoxia Green Reagent for Flow Cytometry (Thermo Fisher), which is fluorogenic at low O<sub>2</sub> levels but non-fluorescent under normoxia. As indicated by flow cytometric analysis (Figures 5A–5C, Tables S2 and S3), under hypoxia (1.5% O<sub>2</sub>), the 3ADI-Mb-TATA549-treated group contained significantly less hypoxic cells and decreased fluorescence compared with those of the other groups, including the no-treatment control group, thus confirming the successful delivery of O<sub>2</sub> by the 3ADI-Mb-TATA549 particles. Furthermore, the supply of O<sub>2</sub> by 3ADI-Mb-TATA549 was dose dependent, providing the support for its ability to store and deliver O<sub>2</sub> (Figures 5D–5F). Notably, free Mb protein was unable to increase the intracellular O<sub>2</sub> level of A549 cells under hypoxia (Figures 5A–5C, Tables S2 and S3), presumably due to its inability to penetrate A549 cells and its instability in aqueous solution (Figure 1F). Similar results were also observed when the experiments were conducted under 0.5% O<sub>2</sub>, further confirming the effectiveness of 3ADI-Mb-TATA549 particles in O<sub>2</sub> delivery (Figure S6).

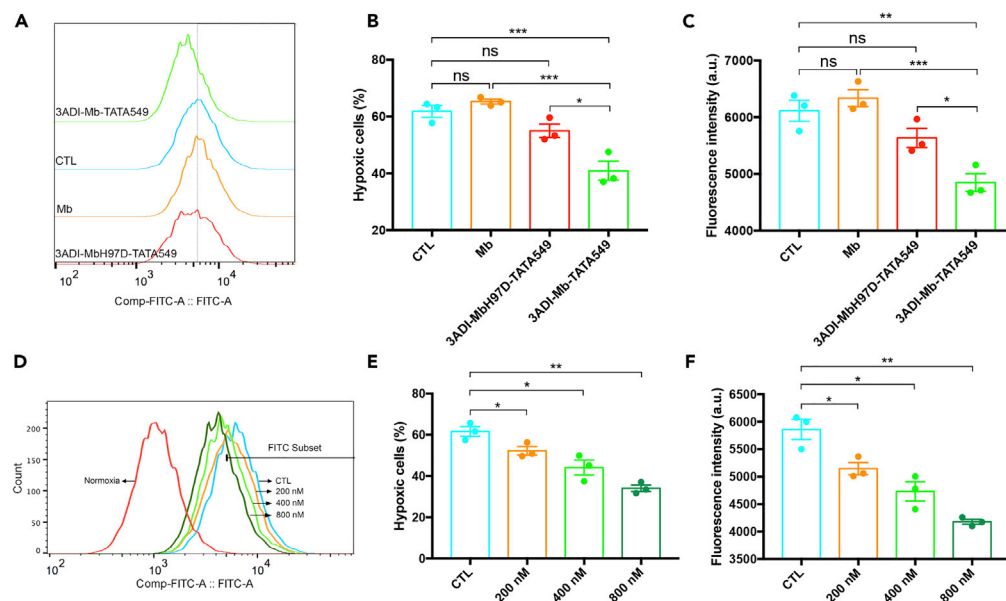


**Figure 5. 3ADI-Mb-TATA549 Particles Increased the Intracellular O<sub>2</sub> Levels of Hypoxic A549 Cells**

(A) Merged flow cytometric histograms showing the decreased fluorescence intensity (more O<sub>2</sub>) of 3ADI-Mb-TATA549-treated hypoxic A549 cells.

(B) Percentage of hypoxic A549 cells exposed to different treatments.

(C) Mean fluorescence intensity of hypoxic A549 cells exposed to different treatments.

(D) Merged flow cytometric histograms of the hypoxic A549 cells treated with different concentrations of 3ADI-Mb-TATA549 particles.

(E) Corresponding bar graphs of 5D showing the percentage of hypoxic cells.

(F) Mean fluorescence intensity illustrating the dose-dependent effects of 3ADI-Mb-TATA549 particles on the O<sub>2</sub> levels of hypoxic A549 cells.

Data are presented as mean ± standard error of the mean. ns: no significant difference; \*p < 0.05; \*\*p < 0.01; \*\*\*p < 0.001.

Having verified that 3ADI-Mb-TATA549 particles were effective in increasing the O<sub>2</sub> level in hypoxic cells, we next analyzed their impact on the susceptibility of A549 cells to radiation. A colony-forming assay was first conducted to verify the protective effect of hypoxia on A549 cells. Cells were incubated either under normoxic (21% O<sub>2</sub>) or hypoxic conditions (1.5% O<sub>2</sub>) for 6 h and then irradiated and re-seeded for colony formation. The surviving fraction (SF) of cells under normoxia after 4 Gy radiation was around 0.04, whereas the SF of cells under hypoxia was 0.27, confirming the increased radioresistance of the hypoxic cells (Figure 6A). The effect of 3ADI-Mb-TATA549 was subsequently investigated by treating A549 cells with 800 nM Mb protein, 3ADI-MbH97D-TATA549 or 3ADI-Mb-TATA549 particles, and then incubating at 37°C under hypoxia (1.5% O<sub>2</sub>) for 6 h, followed by a single dose of irradiation at 4 Gy. As shown in Figures 6B and 6C, the 3ADI-Mb-TATA549-treated cells (SF = 0.17) after exposure to 4 Gy radiation formed significantly fewer colonies compared with the control group (SF = 0.29). Notably, neither free Mb protein (SF = 0.29) nor the mutant 3ADI-MbH97D-TATA549 (SF = 0.28) was able to enhance the susceptibility of hypoxic A549 cells to radiation (Figures 6B and 6C).

Radiation-induced DNA damage initiates cell death mainly by apoptosis (Eriksson and Stigbrand, 2010; Roos and Kaina, 2006). Therefore, to confirm whether the reduced colonies observed for the 3ADI-Mb-TATA549-treated cells was accompanied by an increase in apoptosis, the caspase-3/7 activity of hypoxic A549 cells was measured for the different constructs following irradiation. As expected, cells treated with 3ADI-Mb-TATA549 particles exhibited the highest apoptosis ratio (19.64% apoptotic cells) and caspase-3/7 activity (Figure S7). These results reaffirmed the ability of 3ADI-Mb-TATA549 to effectively deliver O<sub>2</sub> to cells and thereby enhance the sensitivity of radioresistant hypoxic A549 cells to radiotherapy.

## DISCUSSION

The monomeric heme protein myoglobin is expressed predominantly in skeletal and cardiac muscles where it was believed to function solely as an oxygen reservoir, binding O<sub>2</sub> under aerobic conditions

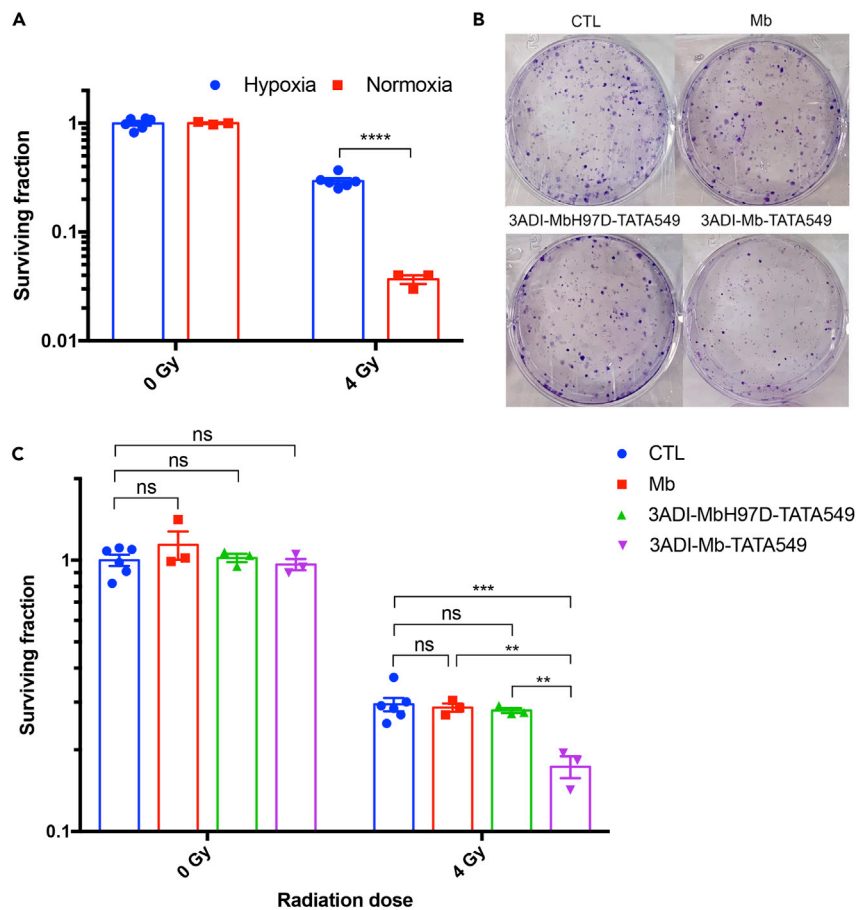


**Figure 6. Effective Delivery of O<sub>2</sub> by 3ADI-Mb-TATA549 Particles Enhanced the Susceptibility of Hypoxia-Induced Radioresistant A549 Cells**

(A) Surviving fractions of A549 cells with or without exposure to radiation under normoxia and hypoxia. Hypoxic cells were significantly more radioresistant than normoxic cells.

(B) Representative images showing the colony formation of hypoxic A549 cells treated with 800 nM Mb protein, 3ADI-MbH97D-TATA549 or 3ADI-Mb-TATA549 protein particles after 4 Gy irradiation.

(C) Quantitative measurements of corresponding surviving fractions of A549 cells in 6B.

Data are presented as mean  $\pm$  standard error of the mean.

ns: no significant difference; \*\*p < 0.01; \*\*\*p < 0.001; \*\*\*\*p < 0.0001.

and releasing it to mitochondria for cellular respiration under hypoxia (Galluzzo et al., 2009; Ordway and Garry, 2004). In recent years, the ectopic expression of myoglobin in non-muscle tissues as well as cancer cell lines and tumors has been reported (Bicker et al., 2020; Flonta et al., 2009; Kristiansen et al., 2011; Meller et al., 2016). Expression profiling of tumors from patients with head and neck squamous cell carcinoma has revealed that myoglobin expression is associated with better prognosis (Meller et al., 2016). The non-canonical tumor suppressor function of myoglobin has also been confirmed by preclinical investigations on breast cancer and lung cancer cells (Braganza et al., 2019; Galluzzo et al., 2009; Kristiansen et al., 2011).

Ample evidence suggests that hypoxia promotes tumor progression and is a potent barrier to effective cancer therapy; thus, overcoming hypoxia is a key element to the successful application of any cancer treatment. In the study by Michieli and colleagues, A549 cells transduced with lentiviral vector-encoding Mb gene exhibited reduced hypoxia and when transplanted into mice delayed tumor engraftment (Galluzzo et al., 2009), suggesting the potential of Mb's ability to conquer tumor hypoxia.

In this study, we took advantage of the high binding affinity of myoglobin for O<sub>2</sub> and its ability to release O<sub>2</sub> under hypoxia to act as an O<sub>2</sub> carrier targeting hypoxia-induced radioresistant cancer cells. We report

the successful proof-of-concept results on the use of our Cry platform to deliver MbO<sub>2</sub> to hypoxic A549 cancer cells as a means to increase the intracellular O<sub>2</sub> levels and thereby enhance their sensitivity to radiation.

One major hurdle to the broad application of protein therapeutics is their instability (Tibbitt et al., 2016). We have previously reported the advantages of the Cry3Aa platform in the immobilization of enzymes and for the delivery of antimicrobial peptides due to its exceptional stability (Heater et al., 2018, 2019; Nair et al., 2015; Yang et al., 2019). Herein we demonstrated the utilization of the crystal-forming domain of Cry3Aa protein to directly produce 3ADI-Mb protein particles in *Bt* cells for myoglobin delivery. Myoglobin within the 3ADI-Mb framework was proven to be more stable than free myoglobin protein. Furthermore, the Cry platform is amenable to modification. Active tumor targeting has shown to improve the specificity of traditional nanomedicine (Danhier, 2016; Danhier et al., 2010). Efficient coupling of functional ligands to the delivery vehicle is therefore crucial to achieve this aim. By simply using recombinant fusion protein technology, the 3ADI platform was further equipped with a cell penetrating peptide TAT and a targeting peptide A549.1 at its C terminus, and the resultant 3ADI-Mb-TATA549 protein particles were directly produced in *Bt*, thus demonstrating the versatility of this platform. It should be noted that the TAT and A549.1 sequences were important in facilitating the facile uptake of 3ADI-Mb-TATA549 protein particles into cells. Since this Cry platform is protein based, the surface-exposed cysteine and lysine residues could also be utilized for chemical conjugation of different ligands, like small molecules, polymers, and peptides.

Numerous studies have shown that many nano/microparticles possess intrinsic properties that induce cytotoxicity in mammalian cells (Fu et al., 2014; Peynshaert et al., 2014), which might also affect their radiosensitivity (Lin et al., 2010; Schaeue and McBride, 2015; Zhuang et al., 2011). Thus, to eliminate any possible effects arising from the particle, rather than the delivered O<sub>2</sub>, we made a 3ADI-MbH97D-TATA549 construct in which His97 of myoglobin was mutated to aspartate to destabilize heme binding, and in turn O<sub>2</sub> binding (Hargrove and Olson, 1996). Unlike 3ADI-Mb-TATA549 particles, delivery of the 3ADI-MbH97D-TATA549 particles to hypoxic A549 cells had minimal effect on the intracellular O<sub>2</sub> levels and radiosensitivity (Figures 5 and 6). These results provide convincing support that 3ADI-Mb-TATA549 protein particles enhance radiotherapy under hypoxia due to its ability to deliver O<sub>2</sub> to hypoxic cancer cells, and not from any particle effects.

Going forward, the next step would be to evaluate the *in vivo* efficacy of 3ADI-Mb-TATA549 particles on a mouse model. To ascertain whether the observed SF decrease (Figure 6C) is sufficient to justify a therapeutic pursuit of this construct on animals or the clinic, we have examined some related studies that reported both *in vitro* and *in vivo* results of radiation. In the work by Grimes et al., nimesulide (Nim) was used to improve the radiation treatment against A549 cells (Grimes et al., 2006). Results from their *in vitro* clonogenic assay showed that the SFs of untreated control and 300 μM Nim group were around 0.4 and 0.2 upon 4 Gy radiation, respectively (Grimes et al., 2006). Consistent with their *in vitro* results, a significant delay of tumor growth was observed for the Nim and radiation combination group compared with that of the radiation-only group in animal models (Grimes et al., 2006). A similar correlation can also be found in the studies by Wolfe et al., in which the SFs of cells treated with goserelin-conjugated gold nanorods (gAuNRs) or PEGylated AuNRs (pAuNRs) upon 4 Gy radiation are around 0.18 and 0.32, respectively (Wolfe et al., 2015). Their *in vivo* results on a mouse xenograft model indicated that the gAuNRs with lower SF significantly improved radiotherapy compared with pAuNRs (Wolfe et al., 2015). In our studies, the SFs of untreated CTL and 3ADI-Mb-TATA549 group were 0.29 and 0.17, respectively, the difference between which is comparable with those reported by the aforementioned studies.

In addition to the clonogenic assay, we have conducted cellular apoptosis assay to investigate the apoptotic effects of the treatment and to corroborate the results of the colony-forming assay. The 3ADI-Mb-TATA549 treatment increased the percentage of caspase 3/7-activated cells from 10% to 20% upon 4 Gy radiation (a 2-fold change) (Figure S7). This 2-fold increase is comparable with that reported by Liu and colleagues, who used perfluorocarbon-loaded hollow Bi<sub>2</sub>Se<sub>3</sub> nanoparticles to enhance radiotherapy (Song et al., 2016). Their *in vitro* experiments showed that the nanoparticles + radiation treatment led to a nearly 2-fold increase in DNA damage compared with radiation alone, and with this degree of difference *in vitro*, they were able to further demonstrate in mouse model that their nanoparticles together with radiation resulted in significant reduction in tumor volume (Song et al., 2016).

We believe all these data should allow us to expect a promising outcome for our construct in animals. Nevertheless, the *in vitro* results, including the SF difference we observed between the CTL and 3ADI-Mb-TATA549, were conducted under specific experimental conditions, and may not be necessarily related to *in vivo* performance. The parameters, including the doses of both particle and radiation, need to be optimized on mice prior to conducting *in vivo* efficacy evaluation experiment.

Another potential concern for the *in vivo* application of the 3ADI-Mb-TATA549 particles is their near-micron size. It has been reported that small nanoparticles (<100 nm) preferentially accumulate in tumor sites by enhanced permeability and retention (EPR) effects, owing to the tumor's leaky vasculature. However, this concept of passive targeting to tumor tissues through EPR effects is still controversial (Danhier, 2016). A recent study showed that inter-endothelial gaps are not responsible for the transport of nanoparticles into solid tumors, whereas up to 97% nanoparticles enter tumors via active transcytosis crossing the tumor endothelium (Sindhvani et al., 2020). This means that the trans-endothelial transport, which is related to the uptake efficiency of particles, is essential to tumor penetration. Given the notable uptake of the 3ADI-Mb-TATA549 particles by mammalian cells, we believe it is possible for them to reach the tumor tissues. There are indeed some studies showing that microparticles could accumulate in tumor (Wang et al., 2020). At present, we think the main hurdle preventing our particles from successful tumor penetration via intravenous (i.v.) injection might be the rapid clearance by the reticuloendothelial system. Some strategies, including PEGylation and modification of particles with "self" peptides, have been developed to abolish the recognition and uptake of particles by phagocytes and therefore prolong their circulation time (Rodriguez et al., 2013; Tong and Kohane, 2016). Given the ease of surface modification of the Cry platform, these approaches can be utilized to improve the *in vivo* performance of our Mb-containing particles for systemic administration. Besides, i.v. injection is not always necessary; microparticles have their own advantages for pulmonary delivery since they can penetrate deep into the lungs (Mitrugotri and Lahann, 2009).

In summary, we have found that the N-terminal helical domain I of Cry3Aa was sufficient to promote the formation of protein inclusions in *Bacillus thuringiensis* cells that stabilized its cargo myoglobin. The addition of tumor targeting and cell penetrating peptide sequences to the Cry-myoglobin fusion protein construct significantly improved cell targeting and uptake efficiency, resulting in increased oxygenation of radioresistant hypoxic cells, thus making them more susceptible to radiation. Our results suggest that the targeted delivery of O<sub>2</sub>-bound myoglobin to increase the intracellular oxygen levels in tumors could be a viable strategy to overcome radioresistance.

### Limitations of the Study

Further *in vivo* investigations on animal models would be needed to study the 3ADI-Mb-TATA549-mediated delivery of O<sub>2</sub> to tumor tissues and its efficiency in improving cancer radiotherapy.

### Resource Availability

#### Lead Contact

Further information and requests for resources and reagents should be directed to the lead contact Prof. Michael K. Chan ([michaelkchan88@cuhk.edu.hk](mailto:michaelkchan88@cuhk.edu.hk)).

#### Materials Availability

Plasmids and protein particles generated in this study will be made available on reasonable requests with a completed Materials Transfer Agreement.

#### Data and Code Availability

The raw data required to reproduce these findings are available from the corresponding authors on reasonable request. The processed data in this study are included in this manuscript and its [Supplemental Information](#) file.

## METHODS

All methods can be found in the accompanying [Transparent Methods supplemental file](#).

## SUPPLEMENTAL INFORMATION

Supplemental Information can be found online at <https://doi.org/10.1016/j.isci.2020.101158>.

## ACKNOWLEDGMENTS

This study was supported by funds from Hong Kong Research Grants Council GRF grant 14121315 (M.K.C. and M.M.M.L.) and the Center of Novel Biomaterials, The Chinese University of Hong Kong (M.K.C.). The funders had no role in study design, data collection and analysis, decision to publish, or preparation of the manuscript. We thank Prof. Didier Lereclus (Institut Pasteur in Paris) and Dr. Daniel Ziegler (*Bacillus* Genetic Stock Center, The Ohio State University) for kindly providing us with the *Bt* strains. We would also like to thank Dr. Manoj S. Nair for constructing the *pHT315-Cry3Aa-myoglobin* plasmid.

## AUTHOR CONTRIBUTIONS

Conceptualization, M.K.C., M.M.M.L., and Z.Y.; Methodology, M.K.C., M.M.M.L., Z.Y., and B.S.H.; Investigation, Z.Y., B.S.H., C.T.C., and A.F.P.; Writing – Original Draft, Z.Y.; Writing – Review & Editing, Z.Y., M.K.C., M.M.M.L., and B.S.H.; Funding Acquisition, M.K.C. and M.M.M.L.; Resources, M.K.C., M.M.M.L., and A.F.P.; Supervision, M.K.C. and M.M.L.

## DECLARATION OF INTERESTS

The authors declare no conflict of interest.

Received: March 4, 2020

Revised: April 24, 2020

Accepted: May 7, 2020

Published: June 26, 2020

## REFERENCES

- Allen, T.M. (2002). Ligand-targeted therapeutics in anticancer therapy. *Nat. Rev. Cancer* 2, 750.
- Barnett, G.C., West, C.M., Dunning, A.M., Elliott, R.M., Coles, C.E., Pharoah, P.D., and Burnet, N.G. (2009). Normal tissue reactions to radiotherapy: towards tailoring treatment dose by genotype. *Nat. Rev. Cancer* 9, 134.
- Bicker, A., Nauth, T., Gerst, D., Aboouf, M.A., Fandrey, J., Kristiansen, G., Gorr, T.A., and Hankeln, T. (2020). The role of myoglobin in epithelial cancers: Insights from transcriptomics. *Int. J. Mol. Med.* 45, 385–400.
- Braganza, A., Quesnelle, K., Bickta, J., Reyes, C., Wang, Y., Jessup, M., Croix, C.S., Arlotti, J., Singh, S.V., and Shiva, S. (2019). Myoglobin induces mitochondrial fusion, thereby inhibiting breast cancer cell proliferation. *J. Biol. Chem.* 294, 7269–7282.
- Brown, J.M., and Wilson, W.R. (2004). Exploiting tumour hypoxia in cancer treatment. *Nat. Rev. Cancer* 4, 437.
- Cheng, Y., Cheng, H., Jiang, C., Qiu, X., Wang, K., Huan, W., Yuan, A., Wu, J., and Hu, Y. (2015). Perfluorocarbon nanoparticles enhance reactive oxygen levels and tumour growth inhibition in photodynamic therapy. *Nat. Commun.* 6, 8785.
- Danhier, F. (2016). To exploit the tumor microenvironment: since the EPR effect fails in the clinic, what is the future of nanomedicine? *J. Control Release* 244, 108–121.
- Danhier, F., Feron, O., and Préat, V. (2010). To exploit the tumor microenvironment: passive and active tumor targeting of nanocarriers for anti-cancer drug delivery. *J. Control Release* 148, 135–146.
- Eriksson, D., and Stigbrand, T. (2010). Radiation-induced cell death mechanisms. *Tumor Biol.* 31, 363–372.
- Flonta, S.E., Arena, S., Pisacane, A., Michieli, P., and Bardelli, A. (2009). Expression and functional regulation of myoglobin in epithelial cancers. *Am. J. Pathol.* 175, 201–206.
- Frankel, A.D., and Pabo, C.O. (1988). Cellular uptake of the tat protein from human immunodeficiency virus. *Cell* 55, 1189–1193.
- Fu, P.P., Xia, Q., Hwang, H.-M., Ray, P.C., and Yu, H. (2014). Mechanisms of nanotoxicity: generation of reactive oxygen species. *J. Food Drug Anal.* 22, 64–75.
- Galluzzo, M., Pennacchietti, S., Rosano, S., Comoglio, P.M., and Michieli, P. (2009). Prevention of hypoxia by myoglobin expression in human tumor cells promotes differentiation and inhibits metastasis. *J. Clin. Invest.* 119, 865–875.
- Green, M., and Loewenstein, P.M. (1988). Autonomous functional domains of chemically synthesized human immunodeficiency virus tat trans-activator protein. *Cell* 55, 1179–1188.
- Grimes, K.R., Warren, G.W., Fang, F., Xu, Y., and St Clair, W.H. (2006). Cyclooxygenase-2 inhibitor, nimesulide, improves radiation treatment against non-small cell lung cancer both *in vitro* and *in vivo*. *Oncol. Rep.* 16, 771–776.
- Gu, Z., Biswas, A., Zhao, M., and Tang, Y. (2011). Tailoring nanocarriers for intracellular protein delivery. *Chem. Soc. Rev.* 40, 3638–3655.
- Hargrove, M.S., and Olson, J.S. (1996). The stability of holomyoglobin is determined by heme affinity. *Biochemistry* 35, 11310–11318.
- Heater, B.S., Chan, W.S., Lee, M.M., and Chan, M.K. (2019). Directed evolution of a genetically encoded immobilized lipase for the efficient production of biodiesel from waste cooking oil. *Biotechnol. Biofuels* 12, 165.
- Heater, B.S., Lee, M.M., and Chan, M.K. (2018). Direct production of a genetically-encoded immobilized biodiesel catalyst. *Sci. Rep.* 8, 12783.
- Huang, C.-C., Chia, W.-T., Chung, M.-F., Lin, K.-J., Hsiao, C.-W., Jin, C., Lim, W.-H., Chen, C.-C., and Sung, H.-W. (2016). An implantable depot that can generate oxygen *in situ* for overcoming hypoxia-induced resistance to anticancer drugs in chemotherapy. *J. Am. Chem. Soc.* 138, 5222–5225.
- Kristiansen, G., Hu, J., Wichmann, D., Stiehl, D.P., Rose, M., Gerhardt, J., Bohnert, A., ten Haaf, A., Moch, H., and Raleigh, J. (2011). Endogenous myoglobin in breast cancer is hypoxia-inducible by alternative transcription and functions to impair mitochondrial activity a role in tumor suppression? *J. Biol. Chem.* 286, 43417–43428.
- Lereclus, D., Agaisse, H., Gominet, M., and Chauvaux, J. (1995). Overproduction of encapsulated insecticidal crystal proteins in a *Bacillus thuringiensis* spoOA mutant. *Nat. Biotechnol.* 13, 67.

- Li, F., Mei, H., Gao, Y., Xie, X., Nie, H., Li, T., Zhang, H., and Jia, L. (2017). Co-delivery of oxygen and erlotinib by aptamer-modified liposomal complexes to reverse hypoxia-induced drug resistance in lung cancer. *Biomaterials* **145**, 56–71.
- Lin, C.-I., Whang, E.E., Donner, D.B., Du, J., Lorch, J., He, F., Jiang, X., Price, B.D., Moore, F.D., and Ruan, D.T. (2010). Autophagy induction with RAD001 enhances chemosensitivity and radiosensitivity through Met inhibition in papillary thyroid cancer. *Mol. Cancer Res.* **8**, 1217–1226.
- Lowe, K.C. (2006). Blood substitutes: from chemistry to clinic. *J. Mater. Chem.* **16**, 4189–4196.
- Luo, Z., Zheng, M., Zhao, P., Chen, Z., Siu, F., Gong, P., Gao, G., Sheng, Z., Zheng, C., and Ma, Y. (2016). Self-monitoring artificial red cells with sufficient oxygen supply for enhanced photodynamic therapy. *Sci. Rep.* **6**, 23393.
- McGuire, M.J., Gray, B.P., Li, S., Cupka, D., Byers, L.A., Wu, L., Rezaie, S., Liu, Y.-H., Pattisapu, N., and Issac, J. (2014). Identification and characterization of a suite of tumor targeting peptides for non-small cell lung cancer. *Sci. Rep.* **4**, 4480.
- Meller, S., Van Ellen, A., Gevensleben, H., Bicker, A., Hankeln, T., Gorr, T.A., Sailer, V., Dröge, F., Schröck, F., and Bootz, F. (2016). Ectopic myoglobin expression is associated with a favourable outcome in head and neck squamous cell carcinoma patients. *Anticancer Res.* **36**, 6235–6241.
- Mitragotri, S., Burke, P.A., and Langer, R. (2014). Overcoming the challenges in administering biopharmaceuticals: formulation and delivery strategies. *Nat. Rev. Drug Discov.* **13**, 655.
- Mitragotri, S., and Lahann, J. (2009). Physical approaches to biomaterial design. *Nat. Mater.* **8**, 15–23.
- Nair, M.S., Lee, M.M., Bonnegarde-Bernard, A., Wallace, J.A., Dean, D.H., Ostrowski, M.C., Burry, R.W., Boyaka, P.N., and Chan, M.K. (2015). Cry protein crystals: a novel platform for protein delivery. *PLoS One* **10**, e0127669.
- Ordway, G.A., and Garry, D.J. (2004). Myoglobin: an essential hemoprotein in striated muscle. *J. Exp. Biol.* **207**, 3441–3446.
- Park, H.-W., and Federici, B.A. (2000). Domain I plays an important role in the crystallization of Cry3A in *Bacillus thuringiensis*. *Mol. Biotechnol.* **16**, 97–107.
- Peynshaert, K., Manshian, B.B., Joris, F., Braeckmans, K., De Smedt, S.C., Demeester, J., and Soenen, S.J. (2014). Exploiting intrinsic nanoparticle toxicity: the pros and cons of nanoparticle-induced autophagy in biomedical research. *Chem. Rev.* **114**, 7581–7609.
- Pratt, C.W., Voet, D., and Voet, J.G. (2008). *Fundamentals of Biochemistry: Life at the Molecular Level*, Third Edition (John Wiley & Sons, Inc.).
- Qin, X., Yu, C., Wei, J., Li, L., Zhang, C., Wu, Q., Liu, J., Yao, S.Q., and Huang, W. (2019). Rational design of nanocarriers for intracellular protein delivery. *Adv. Mater.* **31**, e1902791.
- Riess, J.G. (2006). Perfluorocarbon-based oxygen delivery. *Artif. Cells Blood Subst. Biotechnol.* **34**, 567–580.
- Rodriguez, P.L., Harada, T., Christian, D.A., Pantano, D.A., Tsai, R.K., and Discher, D.E. (2013). Minimal "Self" peptides that inhibit phagocytic clearance and enhance delivery of nanoparticles. *Science* **339**, 971–975.
- Roos, W.P., and Kaina, B. (2006). DNA damage-induced cell death by apoptosis. *Trends Mol. Med.* **12**, 440–450.
- Schaue, D., and McBride, W.H. (2015). Opportunities and challenges of radiotherapy for treating cancer. *Nat. Rev. Clin. Oncol.* **12**, 527.
- Sindhvani, S., Syed, A.M., Ngai, J., Kingston, B.R., Maiorino, L., Rothschild, J., MacMillan, P., Zhang, Y., Rajesh, N.U., and Hoang, T. (2020). The entry of nanoparticles into solid tumours. *Nat. Mater.* **19**, 566–575.
- Song, G., Ji, C., Liang, C., Song, X., Yi, X., Dong, Z., Yang, K., and Liu, Z. (2017a). TaOx decorated perfluorocarbon nanodroplets as oxygen reservoirs to overcome tumor hypoxia and enhance cancer radiotherapy. *Biomaterials* **112**, 257–263.
- Song, G., Liang, C., Yi, X., Zhao, Q., Cheng, L., Yang, K., and Liu, Z. (2016). Perfluorocarbon-loaded hollow Bi<sub>2</sub>Se<sub>3</sub> nanoparticles for timely supply of oxygen under near-infrared light to enhance the radiotherapy of cancer. *Adv. Mater.* **28**, 2716–2723.
- Song, X., Feng, L., Liang, C., Gao, M., Song, G., and Liu, Z. (2017b). Liposomes co-loaded with metformin and chlorin e6 modulate tumor hypoxia during enhanced photodynamic therapy. *Nano Res.* **10**, 1200–1212.
- Sun, W., Lu, Y., and Gu, Z. (2014). Advances in anticancer protein delivery using micro/nanoparticles. *Part. Part. Syst. Charact.* **31**, 1204–1222.
- Sykes, P.A., Shiue, H.-C., Walker, J.R., and Bateman, R.C., Jr. (1999). Determination of myoglobin stability by visible spectroscopy. *J. Chem. Educ.* **76**, 1283.
- Tibbitt, M.W., Dahlman, J.E., and Langer, R. (2016). Emerging frontiers in drug delivery. *J. Am. Chem. Soc.* **138**, 704–717.
- Tong, R., and Kohane, D.S. (2016). New strategies in cancer nanomedicine. *Annu. Rev. Pharmacol. Toxicol.* **56**, 41–57.
- Wang, D., Yao, Y., He, J., Zhong, X., Li, B., Rao, S., Yu, H., He, S., Feng, X., and Xu, T. (2020). Engineered cell-derived microparticles Bi<sub>2</sub>Se<sub>3</sub>/DOX@MPs for imaging guided synergistic photothermal/low-dose chemotherapy of cancer. *Adv. Sci.* **7**, 1901293.
- Wilson, W.R., and Hay, M.P. (2011). Targeting hypoxia in cancer therapy. *Nat. Rev. Cancer* **11**, 393.
- Wolfe, T., Chatterjee, D., Lee, J., Grant, J.D., Bhattarai, S., Tailor, R., Goodrich, G., Nicolucci, P., and Krishnan, S. (2015). Targeted gold nanoparticles enhance sensitization of prostate tumors to megavoltage radiation therapy *in vivo*. *Nanomedicine* **11**, 1277–1283.
- Yang, Z., Zheng, J., Chan, C.-F., Wong, I.L., Heater, B.S., Chow, L.M., Lee, M.M., and Chan, M.K. (2019). Targeted delivery of antimicrobial peptide by cry protein crystal to treat intramacrophage infection. *Biomaterials* **217**, 119286.
- Zhuang, W., Li, B., Long, L., Chen, L., Huang, Q., and Liang, Z. (2011). Induction of autophagy promotes differentiation of glioma-initiating cells and their radiosensitivity. *Int. J. Cancer* **129**, 2720–2731.

**iScience, Volume 23**

**Supplemental Information**

**Targeted Myoglobin Delivery as a Strategy  
for Enhancing the Sensitivity  
of Hypoxic Cancer Cells to Radiation**

**Zaofeng Yang, Bradley S. Heater, Clayton T. Cuddington, Andre F. Palmer, Marianne M.M. Lee, and Michael K. Chan**

SUPPLEMENTAL INFORMATION

SUPPLEMENTAL FIGURES

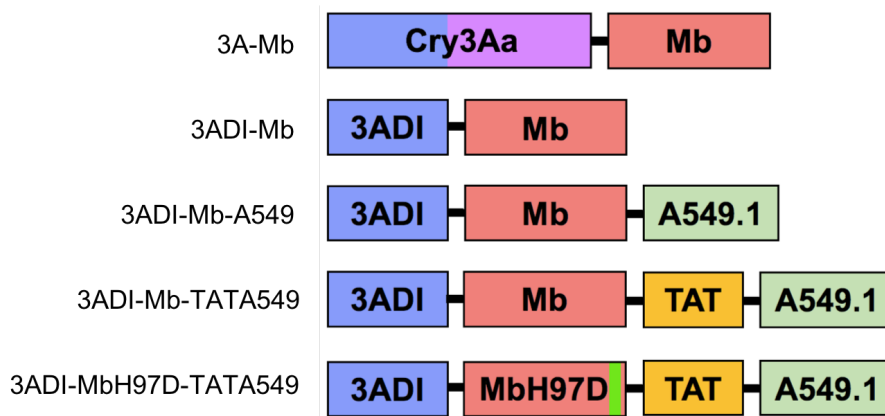


Figure S1. Schematic representation of Mb-containing constructs, Related to Figure 1, Figure 4 and Table 1. 3ADI: Cry3Aa domain I; Mb: myoglobin.

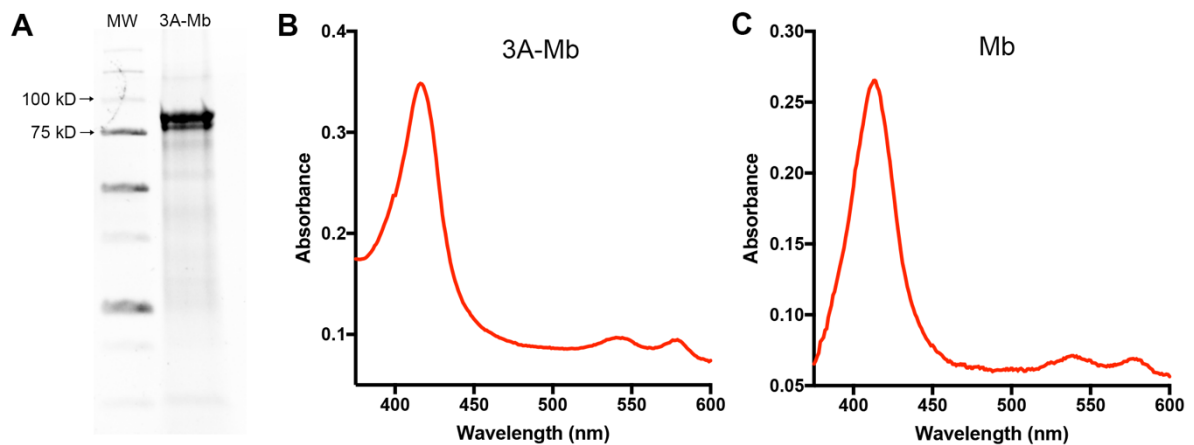
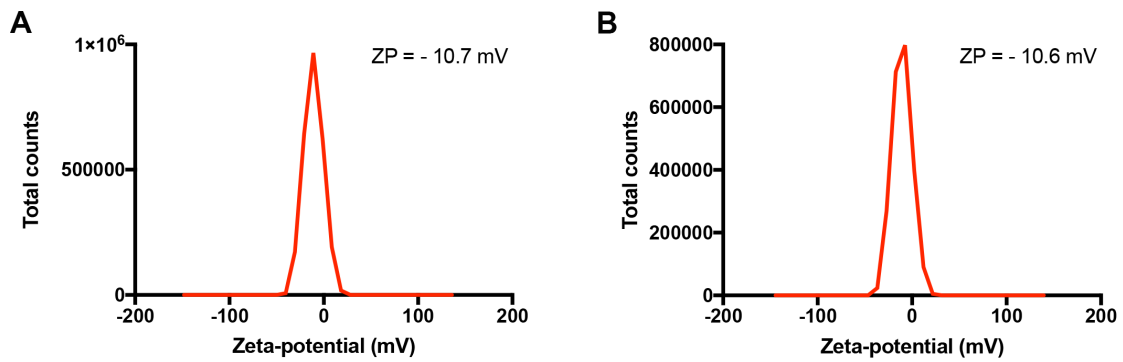
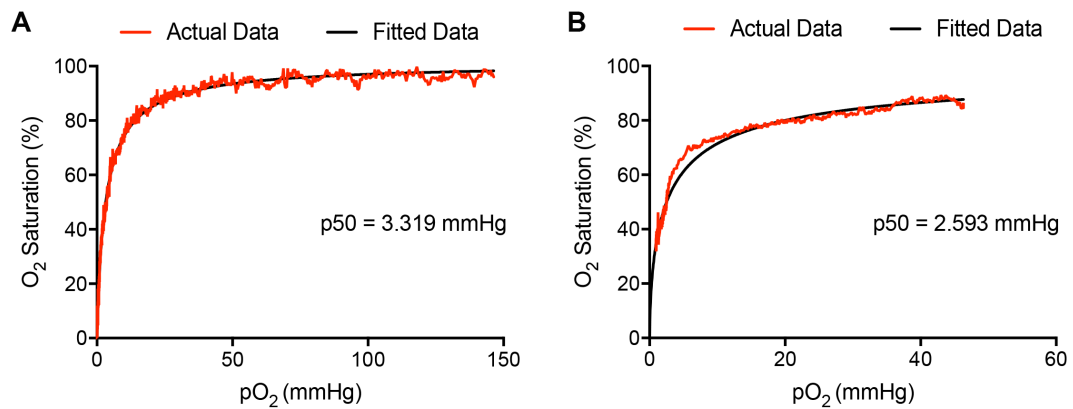


Figure S2. Characterization of 3A-Mb protein particles, Related to Figure 1. (A) SDS-PAGE analysis of purified 3A-Mb protein particles. UV-vis absorption spectra of (B) 3A-Mb particles and (C) wildtype Mb protein.



**Figure S3. Zeta potential distributions of (A) 3ADI-Mb-TATA549 and (B) 3ADI-MbH97D-TATA549 protein particles, Related to Figure 4.**



**Figure S4. Oxygen dissociation spectra of (A) wildtype Mb protein and (B) 3ADI-Mb-TATA549 protein particles, Related to Figure 4.**

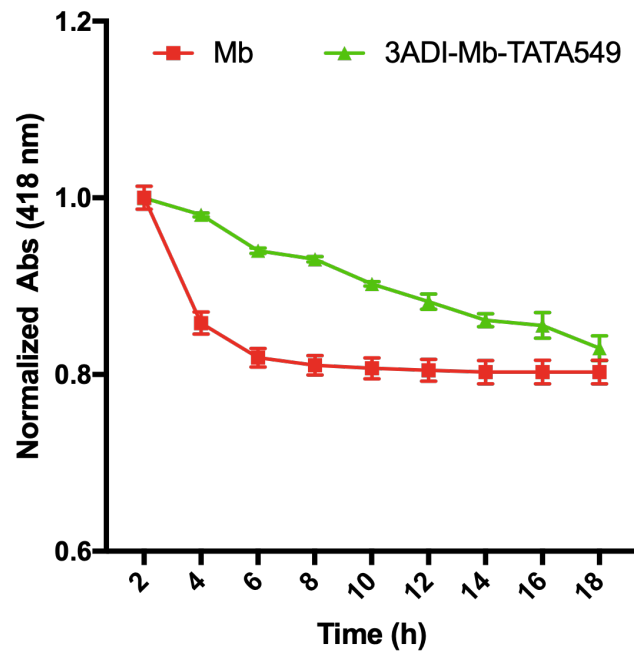


Figure S5. Denaturation profiles of Mb protein and 3ADI-Mb-TATA549 particles, Related to Figure 4.

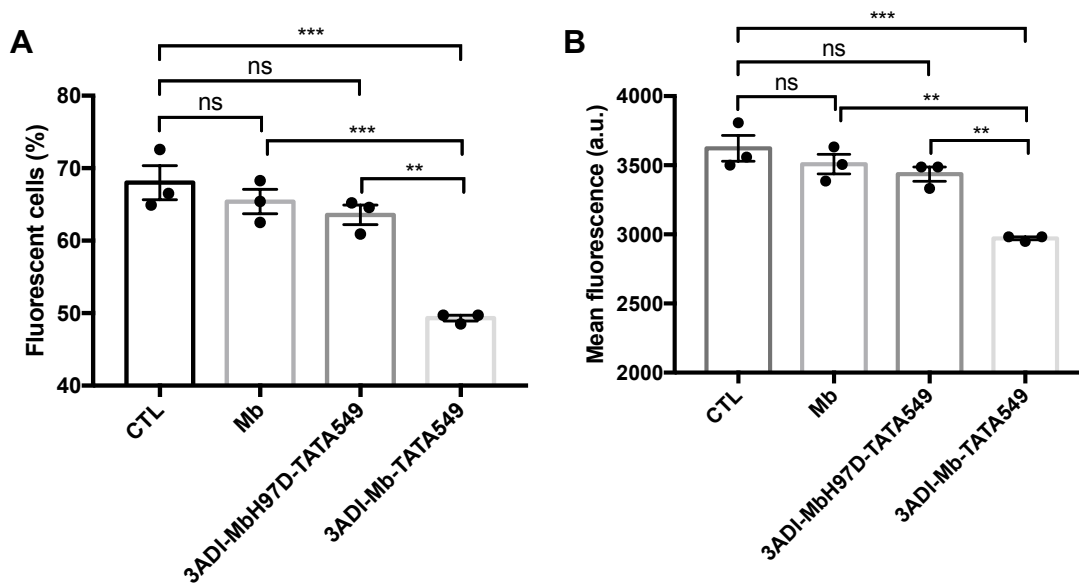


Figure S6. 3ADI-Mb-TATA549 particles increased the intracellular  $O_2$  level of hypoxic A549 cells (0.5%  $O_2$ ), Related to Figure 5.

(A) Percentage of hypoxic A549 cells exposed to different treatments.

(B) Mean fluorescence intensity of hypoxic A549 cells exposed to different treatments.

Data are presented as mean  $\pm$  standard error of the mean.

ns: no significant difference; \*  $P < 0.05$ ; \*\*  $P < 0.01$ ; \*\*\*  $P < 0.001$ ; \*\*\*\*  $P < 0.0001$ .

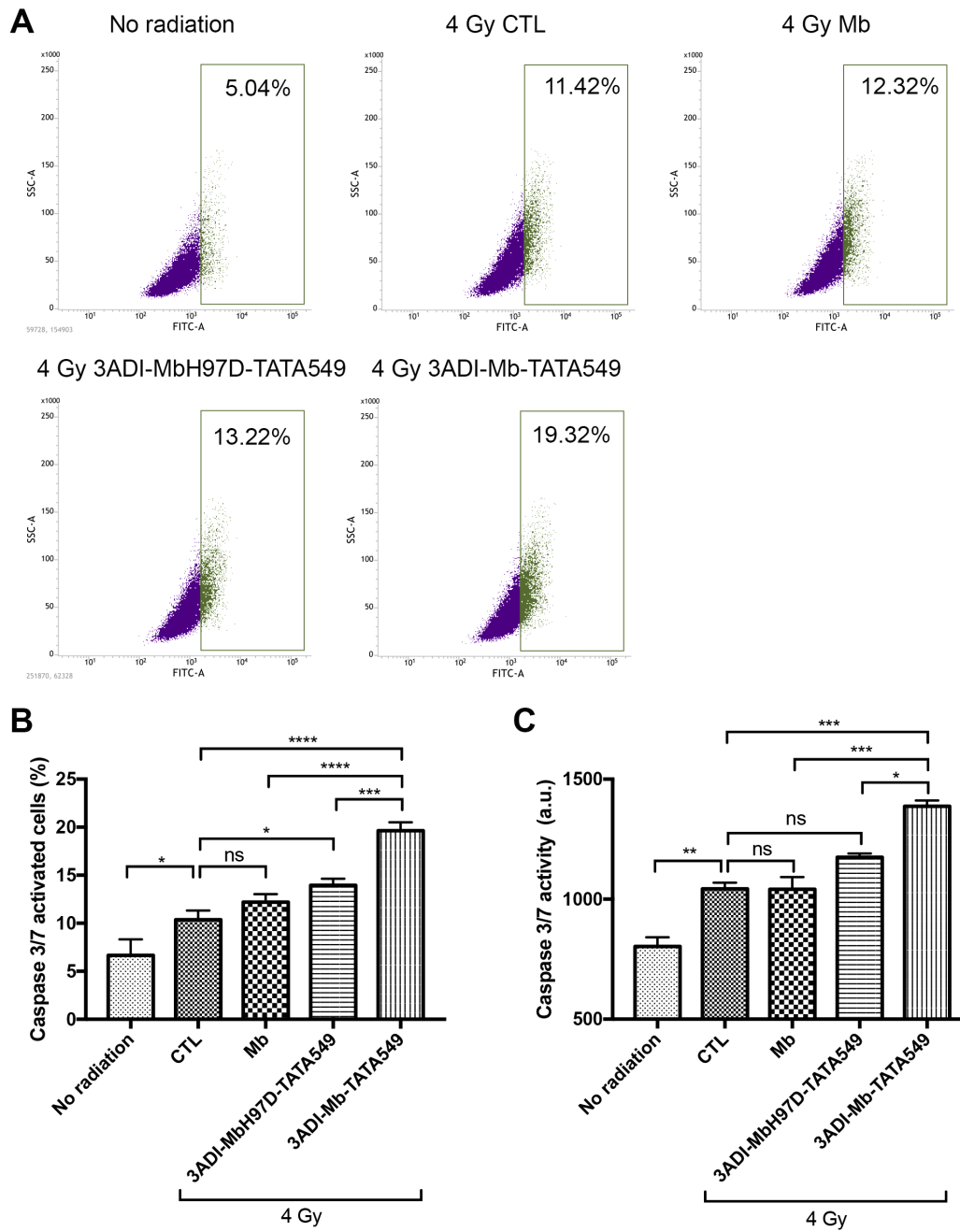


**Figure S7. Caspase-3/7 activities of A549 cells with different treatments post-radiation under hypoxia, Related to Figure 6.** Cells were treated with 800 nM free Mb protein or different Mb-containing particles and incubated under hypoxia (1.5% O<sub>2</sub>) for 6h prior to the 4 Gy radiation. Caspase-3/7 activities were determined by caspase-3/7 green detection reagent 24h after radiation.

(A) Representative flow cytometry dot plots of A549 cells with different treatments. The 3ADI-Mb-TATA549 group displayed more caspase-3/7-activated cells.

(B) Percentage of caspase-3/7 activated cells and (C) their relative caspase-3/7 activity.

Data are presented as mean  $\pm$  standard error of the mean.

ns: no significant difference; \* P < 0.05; \*\* P < 0.01; \*\*\* P < 0.001; \*\*\*\* P < 0.0001.

## SUPPLEMENTAL TABLES

**Table S1. Physical characteristics of Mb-containing particles reported in this paper, Related to Figure 1 and Figure 4.**

	MW of fusion protein	Particle size (DLS)	Particle size (SEM)	Zeta potential
<b>3A-Mb</b>	90.56 kD	ND*	ND	ND
<b>3ADI-Mb</b>	50.83 kD	886.3 nm	869.22 nm	- 9.94 mV
<b>3ADI-Mb-A549</b>	53.33 kD	ND	ND	ND
<b>3ADI-Mb-TATA549</b>	54.39 kD	630.4 nm	647.71 nm	-10.7 mV
<b>3ADI-MbH97D-TATA549</b>	54.37 kD	655.1 nm	658.55 nm	-10.6 mV

\*ND: Not determined.

**Table S2. Raw data of Figure 5B and corresponding statistical analysis, Related to Figure 5.**

Hypoxic cells (%)				
CTL	Mb	3ADI-MbH97D-TATA549	3ADI-Mb-TATA549	
57.7	63.9	59.6	47.5	
64.4	65.1	53.3	37	
63.3	66.8	52	38.3	
Statistical analysis				
ANOVA summary				
F	21.6			
P value	0.0003			
P value summary	***			
Significant diff. among means (P < 0.05)?	Yes			
R square	0.8901			
Tukey's multiple comparisons test	Mean Diff.	95.00% CI of diff.	Summary	Adjusted P Value
CTL vs. Mb	-3.467	-13.95 to 7.018	ns	0.7221
CTL vs. 3ADI-MbH97D-TATA549	6.833	-3.652 to 17.32	ns	0.2357
CTL vs. 3ADI-Mb-TATA549	20.87	10.38 to 31.35	***	0.0010
Mb vs. 3ADI-MbH97D-TATA549	10.3	-0.185 to 20.78	ns	0.0541
Mb vs. 3ADI-Mb-TATA549	24.33	13.85 to 34.82	***	0.0003
3ADI-MbH97D-TATA549 vs. 3ADI-Mb-TATA549	14.03	3.548 to 24.52	*	0.0114

**Table S3. Raw data of Figure 5C and corresponding statistical analysis, Related to Figure 5.**

<b>Mean fluorescence intensity (a.u.)</b>				
CTL	Mb	3ADI-MbH97D-TATA549	3ADI-Mb-TATA549	
5757	6148	5966	5159	
6204	6229	5522	4672	
6381	6630	5410	4713	
<b>Statistical analysis</b>				
ANOVA summary				
F	15.8			
P value	0.0010			
P value summary	**			
Significant diff. among means (P < 0.05)?	Yes			
R square	0.8556			
Tukey's multiple comparisons test				
	Mean Diff.	95.00% CI of diff.	Summary	Adjusted P Value
CTL vs. Mb	-221.7	-972.1 to 528.7	ns	0.7821
CTL vs. 3ADI-MbH97D-TATA549	481.3	-269.1 to 1232	ns	0.2461
CTL vs. 3ADI-Mb-TATA549	1266	515.6 to 2016	**	0.0029
Mb vs. 3ADI-MbH97D-TATA549	703	-47.41 to 1453	ns	0.0665
Mb vs. 3ADI-Mb-TATA549	1488	737.3 to 2238	***	0.0010
3ADI-MbH97D-TATA549 vs. 3ADI-Mb-TATA549	784.7	34.26 to 1535	*	0.0407

## TRANSPARENT METHODS

### KEY RESOURCES TABLE

REAGENT or RESOURCE	SOURCE	IDENTIFIER
<b>Bacterial and Virus Strains</b>		
<i>Bacillus thuringiensis</i> 407-OA	Dr. Daniel Ziegler <i>Bacillus</i> Genetic Stock Center, The Ohio State University	N/A
<i>E. coli</i> XL10-Gold	Dr. Tien-Hsien Chang Genomics Research Center, Academia Sinica	N/A
<i>E. coli</i> BL21 (DE3)	Dr. Shannon Au The Chinese University of Hong Kong	N/A
<b>Chemicals, Peptides, and Recombinant Proteins</b>		
Alexa Fluor™ 488 C <sub>5</sub> Maleimide	Thermo Fisher	Cat. No.: A10254
Wheat Germ Agglutinin Alexa Fluor™ 647 conjugate	Thermo Fisher	Cat. No.: W32466
Hoechst 33342	Thermo Fisher	Cat. No.: 62249
Hypoxia Green Reagent for Flow Cytometry	Thermo Fisher	Cat. No.: H20035
5-Aminolevulinic Acid Hydrochloride Salt	Santa Cruz	Cat. No.: SC-262399
Crystal violet	Sigma-Aldrich	Cat No.: C0775
<b>Critical Commercial Assays</b>		
CellEvent™ Caspase-3/7 Green Flow Cytometry Assay Kit	Thermo Fisher	Cat. No.: C10427
<b>Experimental Models: Cell Lines</b>		
Adenocarcinomic alveolar basal epithelial A549 cells	Dr. M.C. Fung The Chinese University of Hong Kong	N/A
Human gastric epithelial GES-1 cells	Dr. C.H. Cho The Chinese University of Hong Kong	N/A
<b>Recombinant DNA</b>		
Sperm whale myoglobin (pMb413) plasmid	Springer and Sligar, 1987.	Addgene plasmid #20058
pHT315- <i>cry3Aa-Mb</i> plasmid	This paper	N/A
pHT315- <i>cry3AaDI-gfp</i> plasmid	This paper	N/A
pHT315- <i>cry3AaDI-gfp-A549</i> plasmid	This paper	N/A
pHT315- <i>cry3AaDI-Mb</i> plasmid	This paper	N/A
pHT315- <i>cry3AaDI-Mb-A549</i> plasmid	This paper	N/A
pHT315- <i>cry3AaDI-Mb-TATA549</i> plasmid	This paper	N/A
pHT315- <i>cry3AaDI-MbH97D-TATA549</i> plasmid	This paper	N/A
<b>Software and Algorithms</b>		
Flowjo 10.4	BD	N/A
Prism 7	GraphPad	N/A

### EXPERIMENTAL MODEL AND SUBJECT DETAILS

A549 cells were maintained in F-12K medium supplemented with 10% FBS, 1× P/S and 1:5000 Gentamicin. GES-1 cells were maintained in DMEM medium supplemented with 10% FBS and 1× P/S. Cells were maintained at 37°C in a humidified incubator containing 5% CO<sub>2</sub>.

## METHOD DETAILS

### Expression and purification of myoglobin protein

The pMb413 plasmid harboring the gene encoding myoglobin protein was transformed into *E. coli* strain BL21 (DE3). Transformed colonies were inoculated into 700 mL LB (IBI Scientific) supplemented with 50 µg/mL ampicillin and grown overnight at 37°C, with shaking at 220 rpm. The cells were harvested at 8,000 rpm for 7 min, resuspended in buffer A (40 mM sodium citrate pH 5.0) supplemented with 2 mM benzamidine hydrochloride (Benz-HCl, TCI Chemicals) and lysed by sonication. The cell lysate was clarified by centrifugation and total protein was loaded onto a 5-mL HiTrap CM FF column (GE) and washed with 50 mL buffer A. The Mb protein was eluted using a linear gradient of Buffer B (50 mM Tris-HCl, 60 mM NaCl, pH 8.8) and the purity of Mb in each elution fraction was analyzed by SDS-PAGE.

### Expression and purification of different protein particles

Individual genes encoding the sperm whale myoglobin (*Mb*), the green fluorescent protein (*gfp*), the green fluorescent protein modified with a C-terminal A549.1 peptide (*gfp-A549*), the myoglobin protein modified with a C-terminal A549.1 peptide (*Mb-A549*) and the myoglobin protein modified with a C-terminal TAT and A549.1 peptides (*Mb-TATA549*) were amplified by PCR and inserted downstream of the *cry3Aa* or *cry3AaDI* gene in the pHT315 vector via GIBSON Assembly (NEB). The H97D mutation was introduced into the pHT315-*cry3AaDI-Mb-TATA549* plasmid by site-directed mutagenesis using the PfuTurbo DNA polymerase (Agilent) and the mutagenic primers containing the corresponding mutations. To produce the protein inclusions of interest in *Bt*, pHT315-*cry3Aa-Mb*, pHT315-*cry3AaDI-gfp*, pHT315-*cry3AaDI-gfp-A549*, pHT315-*cry3AaDI-Mb*, pHT315-*cry3AaDI-Mb-A549*, pHT315-*cry3AaDI-Mb-TATA549* or pHT315-*cry3AaDI-MbH97D-TATA549* plasmids were transformed into *Bt* 407-OA cells by electroporation following the procedures as previously described (Nair et al., 2015; Yang et al., 2019). Specifically, for the production of fusion inclusions containing myoglobin, 0.2 mM 5-aminolevulinic acid (ALA), a heme precursor, was added to the culture medium to boost heme synthesis. Protein particles were isolated by sucrose gradient centrifugation. The purity of purified protein particles was examined using phase contrast microscope and analyzed by SDS-PAGE.

### Functional analyses of free Mb protein and Mb-contained protein particles

Purified 3A-Mb, 3ADI-Mb, 3ADI-Mb-TATA549 and 3ADI-MbH97D-TATA549 protein particles were resuspended in ddH<sub>2</sub>O. UV-Vis absorption spectra of Mb protein and these protein particles were obtained by measuring the absorbance from 375 nm to 650 nm in a 96-well plate (Nunc) using an Infinite® M1000 pro (TECAN) spectrophotometer. Oxygen dissociation curves of Mb protein and 3ADI-Mb-TATA549 particles were generated using the HEMOX analyzer (TCS Scientific), and the p50 and Hill coefficients were determined using the Hemox analytical software.

### Stability of Mb protein, 3ADI-Mb and 3ADI-MbTATA549 protein particles

0.45 mg/mL Mb protein, 3ADI-Mb protein particles or 3ADI-Mb-TATA549 protein particles were incubated in 200 µL PBS in a 96-well plate (Nunc) at 37°C. The absorbance at 418 nm was measured every 2 h up to 18 h using an Infinite® M1000 pro (TECAN) spectrophotometer.

### Evaluating the targeting efficiency of the TP A549.1 peptide

A549 cells and GES-1 cells were seeded at 75,000 cells/well in 12-well plates and incubated overnight at 37°C, 5% CO<sub>2</sub> to allow for adherence. Cells were then washed with 1× PBS to remove non-adherent cells, followed by incubation with 100 nM Cry3AaDI-GFP or Cry3AaDI-GFP-A549 protein particles for 24 h. At the end of the incubation period, cells were washed 3 times with PBS to remove non-bound particles and trypsinized for flow cytometric analysis on a BD FACSVerser flow cytometer.

### Scanning electron microscopy

3ADI-Mb, 3ADI-Mb-TATA549 and 3ADI-MbH97D-TATA549 protein particles were resuspended in ddH<sub>2</sub>O (0.4 mg/mL) and 2 µL of the suspension was added to a copper stub and air-dried. Samples were coated with gold by a Sputter Coater S150B (Edwards) and imaged in a SU8000 (Hitachi) scanning electron microscope operated at 5 kV and a working distance of 8.5 mm.

### **Measurements of hydrodynamic diameter and zeta potential**

The hydrodynamic diameter and zeta potential of 3ADI-Mb, 3ADI-Mb-TATA549 and 3ADI-MbH97D-TATA549 protein particles were measured at 25°C using Malvern Zetasizer Nano ZS90. Particles were prepared at 80 µg/mL in ddH<sub>2</sub>O for size measurement and in 1× PBS for zeta potential measurement.

### **Targeting and cellular uptake efficiency of 3ADI-Mb-TATA549 protein particles**

Purified 3ADI-Mb, 3ADI-Mb-A549 or 3ADI-Mb-TATA549 protein particles were labeled with Alexa Fluor™ 488 C<sub>5</sub> Maleimide dye (Thermo Fisher) following manufacturer's protocol. Labeled particles were washed with 1× PBS to remove the excess dye. For the quantitative measurement of the targeting efficiency of A549.1 peptide, A549 cells were seeded on 12-well plates (75,000 cells/well) and incubated overnight at 37°C, 5% CO<sub>2</sub>. Cells were then washed with 1× PBS to remove non-adherent cells and incubated with 200 nM Alexa 488-labeled 3ADI-Mb, Alexa 488-labeled 3ADI-Mb-A549 or Alexa 488-labeled 3ADI-Mb-TATA549 protein particles. After 16 h incubation, cells were washed with 1× PBS (with 20 U/mL heparin) for 3 times and trypsinized for flow cytometric analysis on a BD FACSVerser flow cytometer.

Confocal studies were also performed to evaluate the targeting and uptake efficiency of 3ADI-Mb-TATA549 particles to A549 cells. Briefly, 1 × 10<sup>5</sup> cells/well A549 cells were seeded in a 35-mm confocal dish (MatTek) and incubated at 37°C overnight. Cells were washed with 1× PBS and incubated with 20 nM Alexa 488-labeled 3ADI-Mb, Alexa 488-labeled 3ADI-Mb-A549 or Alexa 488-labeled 3ADI-Mb-TATA549 protein particles for 20 h. At the end of incubation, cells were stained with 0.2 µg/mL Hoechst 33342 (Life Technologies) and 10 µg/mL Wheat Germ Agglutinin Alexa Fluor™ 647 Conjugate (Thermo Fisher) for 10 min, and washed 3 times with 20 U/mL heparin in PBS. Images of A549 cells treated with different particles were captured using a Leica SP8 confocal microscope.

### **Detection of the intracellular O<sub>2</sub> level of A549 cells**

Hypoxia Green Reagent (Thermo Fisher), which releases rhodamine as a result to decreased oxygen levels, was used to ascertain the effects of different doses of 3ADI-Mb-TATA549 protein particle on the intracellular O<sub>2</sub> levels of A549 cells. A549 cells were seeded on 24-well plates (75,000 cells/well) and incubated overnight at 37°C, 5% CO<sub>2</sub>. Cells were then washed with 1× PBS to remove non-adherent cells, treated with different concentrations (200 - 800 nM) of 3ADI-Mb-TATA549 particles, and incubated at 37°C under 1.5% O<sub>2</sub> for 3 h. 0.5 µL of 1 mM Hypoxia Green Reagent was then added into 500 µL culture medium, and cells were further incubated under 1.5% O<sub>2</sub> for another 3 h. At the end of the 6 h incubation, A549 cells were washed and trypsinized for flow cytometric analysis using a BD FACSVerser flow cytometer. For the comparison of 3ADI-Mb-TATA549 particles with free Mb protein and 3ADI-MbH97D-TATA549 protein particles, 800 nM of the respective protein/protein particles were used instead.

### **Colony forming assay**

A549 cells were seeded in 4-well plates (75,000 cells/well) and incubated overnight at 37°C, 5% CO<sub>2</sub>. Cells were then washed with 1× PBS to remove non-adherent cells, and treated with 800 nM free Mb, 3ADI-Mb-TATA549 or 3ADI-MbH97D-TATA549 protein particles. The treated cells, as well as the no treatment control cells, were then incubated under normoxia (21% O<sub>2</sub>) or hypoxia (1.5% O<sub>2</sub>) for 6 h. Cells were next irradiated under the same O<sub>2</sub> levels as their culturing conditions at 4 Gy using a Nordion Gammacell 3000 irradiation system (source: Cesium 137). After irradiation, cells were incubated at normal culture condition (21% O<sub>2</sub>) for 1 h. At the end of incubation period, cells were washed, trypsinized and seeded into 6-well plates (0 Gy: 400 cells/well; 4 Gy: 1500 cells/well) to allow the formation of colonies for 7 days under normal cell culture condition (37°C, 5% CO<sub>2</sub>). Colonies were stained with 2% crystal violet (Sigma-Aldrich) solution in 100% ethanol for 20 min and washed with flowing water. Colonies of at least 50 cells were counted, and the plating efficiency (PE) and surviving fraction (SF) were calculated using the following equation (Franken et al., 2006):

$$PE = (\text{No. of colonies formed} / \text{No. of cells seeded}) \times 100\%$$

$$SF = [\text{No. of colonies formed after treatment} / (\text{No. of cells seeded} \times PE)] \times 100\%.$$

### **Caspase 3/7 activity**

A549 cells were seeded in 4-well plates at 50,000 cells/well and incubated at 37°C, 5% CO<sub>2</sub> to allow the attachment of cells. After overnight incubation, cells were washed with 1× PBS to remove non-adherent cells, treated with 800 nM free Mb protein, 3ADI-Mb-TATA549 or 3ADI-MbH97D-TATA549 protein particles and incubated in a hypoxia incubator (1.5% O<sub>2</sub>) for 6 h. Cells were next irradiated at

4 Gy using a Nordion Gammacell 3000 irradiation system (source: Cesium 137). After irradiation, cells were incubated at 37°C under normoxic conditions for 24 h. At the end of incubation period, cells were washed, trypsinized and stained with CellEvent® Caspase-3/7 Green Detection Reagent (37°C, 30min) for flow cytometric analysis.

### QUANTIFICATION AND STATISTICAL ANALYSIS

Data are presented as mean ± standard error of the mean. Statistical significance and the number of samples are noted in figure legends where appropriate. Intergroup differences were assessed by one-way ANOVA or Student's *t*-test using Prism GraphPad 7.0 software. A value of  $P < 0.05$  was considered significant (\*  $P < 0.05$ , \*\*  $P < 0.01$ , \*\*\*  $P < 0.001$ , \*\*\*\*  $P < 0.0001$ ).

### AMINO ACID SEQUENCES OF DIFFERENT CRY-MB FUSION PROTEINS

#### 3A-Mb

MNPNNRSEHDTIKTTENNEVPTNHVQYPLAETPNPTLEDLNYKEFLRMTADNNTEALDSSTTKDVIQKGISVVGDL  
LLGVVGFPPFGALVSFYTNFLNTIWPSEDPWKAFMEQVEALMDQKIADYAKNKALAEQGLQNNVEDYVSALSSW  
QKNPVSSRNPHSQGRIRELFSQAESHFRNSMPSFAISGYEVLFLTTYAQAANTHLFLLKDAQIYGEWGYEKEDI  
AEFYKRQLKLTQEYTDHCVKWYNVGLDKLRGSSYESWVNFNRYRREMTLTVLDLIALFPLYDVRLYPKEVKTELT  
RDVLTDPDIVGVNLRGYGTTFSNIENYIRKPHLFDYLHRIQFHTRFQPGYGNDSFNYSWGSNYVSTRPSIGSNDI  
ITSPFYGNKSSEPQVQNFENGEKVYRAVANTNLAVWPSAVYSGVTKVEFSQYNDQTDASTQTYDSKRNVGAVSW  
DSIDQLPPETTDEPLEKGYSHQLNYVMCFMQGSRGTIPVLTWTHKSVDFNMIDSKKITQLPLVKAYKLQSGAS  
VVAGPRFTGGDIIQCTENGSAAIYVTPDVSYSQYRARIHYASTSQITFTLSLDGAPFNQYYFDKTINKGDTLT  
YNSFNLASFSTPFELSGNNLQIGVTGLSAGDKVYIDKIEFIPVNGSMVLSEGEWQLVHLHVWAKVEADVAGHGQDI  
LIRLFKSHPETLEKFDKFKHLKTEAEMKASEDLKKGVTVLTALGAILKKKGHHEAELKPLAQSHATKHKIPIKY  
LEFISEAIHVLHSRHPGNFGADAQGAMNKALELFRKDIAAKYKELGYQG

#### 3ADI-Mb

MNPNNRSEHDTIKTTENNEVPTNHVQYPLAETPNPTLEDLNYKEFLRMTADNNTEALDSSTTKDVIQKGISVVGDL  
LLGVVGFPPFGALVSFYTNFLNTIWPSEDPWKAFMEQVEALMDQKIADYAKNKALAEQGLQNNVEDYVSALSSW  
QKNPVSSRNPHSQGRIRELFSQAESHFRNSMPSFAISGYEVLFLTTYAQAANTHLFLLKDAQIYGEWGYEKEDI  
AEFYKRQLKLTQEYTDHCVKWYNVGLDKLRGSSYESWVNFNRYRREMTLTVLDLIALFPLYDVRLGSMVLSEGEW  
QLVHLHVWAKVEADVAGHGQDILIRLFKSHPETLEKFDKFKHLKTEAEMKASEDLKKGVTVLTALGAILKKKGHH  
EAELKPLAQSHATKHKIPIKYLEFISEAIHVLHSRHPGNFGADAQGAMNKALELFRKDIAAKYKELGYQG

#### 3ADI-Mb-A549

MNPNNRSEHDTIKTTENNEVPTNHVQYPLAETPNPTLEDLNYKEFLRMTADNNTEALDSSTTKDVIQKGISVVGDL  
LLGVVGFPPFGALVSFYTNFLNTIWPSEDPWKAFMEQVEALMDQKIADYAKNKALAEQGLQNNVEDYVSALSSW  
QKNPVSSRNPHSQGRIRELFSQAESHFRNSMPSFAISGYEVLFLTTYAQAANTHLFLLKDAQIYGEWGYEKEDI  
AEFYKRQLKLTQEYTDHCVKWYNVGLDKLRGSSYESWVNFNRYRREMTLTVLDLIALFPLYDVRLGSMVLSEGEW  
QLVHLHVWAKVEADVAGHGQDILIRLFKSHPETLEKFDKFKHLKTEAEMKASEDLKKGVTVLTALGAILKKKGHH  
EAELKPLAQSHATKHKIPIKYLEFISEAIHVLHSRHPGNFGADAQGAMNKALELFRKDIAAKYKELGYQGGGGG  
GGSMTVCNASQRQAHAQATAVSL

#### 3ADI-Mb-TATA549

MNPNNRSEHDTIKTTENNEVPTNHVQYPLAETPNPTLEDLNYKEFLRMTADNNTEALDSSTTKDVIQKGISVVGDL  
LLGVVGFPPFGALVSFYTNFLNTIWPSEDPWKAFMEQVEALMDQKIADYAKNKALAEQGLQNNVEDYVSALSSW  
QKNPVSSRNPHSQGRIRELFSQAESHFRNSMPSFAISGYEVLFLTTYAQAANTHLFLLKDAQIYGEWGYEKEDI  
AEFYKRQLKLTQEYTDHCVKWYNVGLDKLRGSSYESWVNFNRYRREMTLTVLDLIALFPLYDVRLGSMVLSEGEW  
QLVHLHVWAKVEADVAGHGQDILIRLFKSHPETLEKFDKFKHLKTEAEMKASEDLKKGVTVLTALGAILKKKGHH  
EAELKPLAQSHATKHKIPIKYLEFISEAIHVLHSRHPGNFGADAQGAMNKALELFRKDIAAKYKELGYQGGGGG  
GGSRRQRKRKGMTCNASQRQAHAQATAVSL

#### 3ADI-MbH97D-TATA549

MNPNNRSEHDTIKTTENNEVPTNHVQYPLAETPNPTLEDLNYKEFLRMTADNNTEALDSSTTKDVIQKGISVVGDL  
LLGVVGFPPFGALVSFYTNFLNTIWPSEDPWKAFMEQVEALMDQKIADYAKNKALAEQGLQNNVEDYVSALSSW  
QKNPVSSRNPHSQGRIRELFSQAESHFRNSMPSFAISGYEVLFLTTYAQAANTHLFLLKDAQIYGEWGYEKEDI  
AEFYKRQLKLTQEYTDHCVKWYNVGLDKLRGSSYESWVNFNRYRREMTLTVLDLIALFPLYDVRLGSMVLSEGEW  
QLVHLHVWAKVEADVAGHGQDILIRLFKSHPETLEKFDKFKHLKTEAEMKASEDLKKGVTVLTALGAILKKKGHH  
EAELKPLAQSHATKHKIPIKYLEFISEAIHVLHSRHPGNFGADAQGAMNKALELFRKDIAAKYKELGYQGGGGG  
GGSRRQRKRKGMTCNASQRQAHAQATAVSL

## REFERENCE

Franken, N.A., Rodermond, H.M., Stap, J., Haveman, J., and Van Bree, C. (2006). Clonogenic assay of cells in vitro. *Nature Protocols* 1, 2315.